The Ursa Major Cluster of Galaxies; 2, Bimodality of the Distribution of Central Surface Brightnesses

Tully, R. B.; Verheijen, M. A. W.

Published in:
The Astrophysical Journal

DOI:
10.1086/304318

The Ursa Major Cluster of Galaxies. II. Bimodality of the Distribution of Central Surface Brightnesses

R. Brent Tully[1] and Marc A.W. Verheijen[2]

[1] Institute for Astronomy, University of Hawaii, 2680 Woodlawn Drive, Honolulu, HI 96822
e-mail: tully@ifa.hawaii.edu

[2] Kapteyn Astronomical Institute, Postbus 800, NL-9700 AV Groningen, The Netherlands
e-mail:verheyen@astro.rug.nl

ABSTRACT— The Ursa Major Cluster appears to be unevolved and made up of HI-rich spiral galaxies like one finds in the field. B, R, I, K' photometry has been obtained for 79 galaxies, including 62 in a complete sample with $M_B^{b,i} < -16.5^m$ (with a distance to the cluster of 15.5 Mpc). The K' information is particularly important for the present discussion because it is not seriously affected by obscuration. There is reasonably convincing evidence that the distribution of exponential disk central surface brightnesses is *bimodal*. There is roughly an order of magnitude difference in the mean luminosity densities of high and low surface brightness disks. Disks *avoid* the domain between the high and low surface brightness zones. The few intermediate surface brightness examples in the sample all have significant neighbors within a projected distance of 80 kpc. The high surface brightness galaxies exhibit a range $-21^m < M_B^{b,i} < -17^m$ while the low surface brightness galaxies are found with $-19^m < M_B^{b,i}$ down to the completion limit. High and low surface brightness galaxies in the overlap regime $-19^m < M_B^{b,i} < -17^m$ that are indistinguishable in luminosity–line width plots have very distinct locations in surface brightness–scale length plots. The existence of separate high and low surface brightness families suggests that there are discrete radial configurations that are stable. Galaxies are driven into one of these regimes. The high surface brightness state has a lower luminosity cutoff. It is likely that the high surface brightness galaxies are dominated by dissipational matter at their centers while the low surface brightness galaxies are dark matter dominated. The high surface brightness family subdivides into those with, and without, substantial bulges. In either case, these galaxies have essentially the same exponential disk central surface brightnesses. Evidently, there are *two thresholds* probably controlled by angular momentum content or transfer. Passing from high to low specific angular momentum, there is first the transition from low surface brightness to high surface brightness regimes, then the transition from exponential disk to disk plus bulge regimes.

1 Freeman's Law

Evidence will be presented that the luminosity densities of the disks of galaxies are bimodally distributed. By inference, the mass densities would also be bimodally distributed. If true, then the distinction between high and low surface brightness systems is a fundamental phenomenon that any theory of galaxy formation should be required to explain.

The surface brightness of galaxy disks falls off exponentially with radius (de Vaucouleurs 1959). Freeman (1970) considered many of the most familiar nearby spiral and S0 galaxies and pointed out that if fits to the main body of disks are extrapolated to the centers then the central surface brightnesses have values in the B band of $\mu_0^B \simeq 21.65$ magnitudes per square arcsec with a very small dispersion. Today many exceptions are known to Freeman's law, inevitably on the low surface brightness side. It has been argued that the constancy of central surface brightness values was an artifact either of obscuration (Jura 1980), or of bulge-disk decomposition methods (Kormendy 1977), or of selection effects that narrow the range of observed surface brightnesses (Disney 1976; Allen & Shu 1979). Van der Kruit (1987) made a strong case for a peak in agreement with Freeman's discovery, although he appreciated that there are low surface brightness galaxies that are discordant. The current dominant point-of-view is that there is a rather flat distribution of central surface brightnesses from $\mu_0^B \sim 20$ down to the faintest accessible levels (McGaugh, Bothun, & Schombert 1995; McGaugh 1996; de Jong 1996*a*). The details of this distribution have not been well determined because of selection effects.

Wide field photographic surveys select for high surface brightness galaxies within a preferred 'visibility' window, in the vocabulary of Disney & Phillipps (1983). Special efforts are necessary to find low surface brightness objects (Impey, Bothun, & Malin 1988; Irwin et al. 1990; Davies et al. 1994; Schwartzenberg et al. 1995). These efforts amply demonstrate the ubiquitousness of low surface brightness galaxies but often the distances to these objects are unknown and it is not easy to achieve a normalization of the counts per surface brightness bin per unit volume element. Going back a bit, the first big compilation of low surface brightness galaxies was by van den Bergh (1959, 1966). Redshifts for these galaxies were obtained by Fisher & Tully (1975) which made it clear that many of the objects in this class are big and intrinsically luminous; the brightest in that sample have $M_B \sim -20$. A big compendium of nearby low surface brightness galaxies is provided by Fisher & Tully (1981). Quite a few samples have been compiled since that time, for example, the new catalog by Impey et al. (1996) which includes objects to $z \sim 0.1$.

This new study contains two observational elements that appear to be important. One is the nature of the sample: we have a statistically significant data set which is *complete to an absolute magnitude limit* drawn from an environment dominated by HI-rich, mostly non-interacting disk galaxies. The other element has to do with the passbands of the photometric material: we combine K' imaging with B, R, I optical imaging.

The raw data has been published in Paper I of this series (Tully et al. 1996). There is a description of the Ursa Major Cluster in that reference. The region is unusual in a favorable way. Clusters are nice because if objects are at a common distance then an *apparent* threshold

corresponds to an *absolute* threshold. However, it is suspected that cluster environments affect the properties of the constituent galaxies, for example, to produce the correlation of galaxy types with local density (Dressler 1980). Yet it was argued in Paper I that the Ursa Major Cluster may be so young that it's members are representative of a 'field' population. The velocity dispersion of the cluster is only 148 km s^{-1}, whence the characteristic crossing time is 0.5 H_0^{-1}. There is no concentration toward a core, no large ellipticals and only a few moderate S0's, and the spirals have normal gas properties. Next to the Virgo Cluster, the Ursa Major Cluster contains by far the largest concentration of spiral galaxies of any bound region in the Local Supercluster. Hence, there is the possibility that all galaxies in the volume of the cluster can be surveyed down to some absolute limit and that these galaxies will be reasonably representative of objects in the low density parts of the universe.

The K' (2.2μm) imaging provides the second important resource for this study. A 256 × 256 HgCdTe detector was used in wide-field modes, providing fields-of-view up to 9 arcmin. The photometry in the infrared is not significantly affected by obscuration and it measures the light from old populations, which is presumably more closely tied to the total mass than the light of young populations.

It has long been appreciated that Freeman's law, if true, provides strong constraints on galaxy formation scenarios. However a galaxy modeler could not be sure if (s)he was being asked to reproduce a real effect or an observational artifact. It is hoped that the present discussion will help revive the focus on an important characteristic of galaxies with the introduction of a couple of curious new elements.

2 Surface Brightness – Scale Length Diagrams

A compilation of photometric data can be found in Paper I for 79 galaxies projected within a 7.5° circle and with $700 < V_{helio} + 300 \sin\ell\cos b < 1210$ km s^{-1}. Of these, 62 galaxies define a *complete sample* with $M_B^{b,i} < -16.5$. CCD B, R, I photometry is available for all 79 galaxies. There is imaging K' photometry available for 60 of the 62 galaxies in the complete sample and for 10 of the 17 fainter galaxies. Absolute magnitudes are based on an assumed distance modulus of 30.95, corresponding to a distance of 15.5 Mpc. Hence, $1'' = 75$ pc. This distance is compatible with a complex velocity field map of the Local Supercluster with a global value of $H_0 = 85$ km s^{-1} Mpc^{-1} (Tully et al. 1997).

2.1 Photometric parameters

One-dimensional projected surface brightness profiles were derived by averaging the surface brightness in concentric ellipses of constant position angle and ellipticity chosen to match the outer isophotes. The surface brightness profiles were fit by a straight line of the form

$$\mu^\lambda(r) = \mu_0^\lambda + 1.086(r/r_d), \tag{1}$$

corresponding to an exponential profile of the form

$$L^{\lambda}(r) = L_0^{\lambda} e^{-r/r_d}. \tag{2}$$

If a bulge was detected, the inner region of the profile was excluded from the fit and μ_0 was determined by extrapolation. Hence, the fall-off of surface brightness with radius $\mu(r)$ in a given passband λ is described by two parameters: the surface brightness at the center of the galaxy μ_0 and the exponential scale length r_d. Typically, 4 to 6 scale lengths are observed above the outer limiting isophot. It is known that giant elliptical galaxies are poorly fit by an exponential form (de Vaucouleurs 1959) but there are no giant ellipticals in the Ursa Major Cluster. There are some moderate luminosity early-type systems that are classified as S0. It is possible to provide at least a crude exponential fit to the main bodies of these galaxies, although inevitably there are substantial bulge components at the centers. It is known that dwarf galaxies, whether irregular or elliptical, can be reasonably approximated by exponential profiles (Binggeli, Sandage, & Tarenghi 1984). Hence, it has been possible to measure the parameters μ_0 and r_d in all available bands for all the galaxies in the sample.

Plots of the positions of galaxies in the domain of these two parameters are informative. We begin in Figure 1 with the directly observed parameters; ie, with no corrections for inclination effects. The solid symbols denote members of the complete sample and the crosses are associated with fainter galaxies. The diagonal lines are loci of constant magnitudes since for an exponential disk

$$m_T^{\lambda} = \mu_0^{\lambda} - 2.5\log 2\pi(b/a) - 5\log r_d. \tag{3}$$

where the observed minor-to-major axial ratio of a galaxy is b/a. The lines are drawn to coincide with the completion boundary, defined in B and roughly transformed to the other bands. The curved lines in the B panel are in the spirit of the visibility limits discussed by Disney & Phillipps (1983). Following from Paper I, the magnitude above the limiting isophote is

$$m_{lim} = m_T - 2.5\log[1 - (1 + \frac{(\mu_{lim} - \mu_0)}{1.086})e^{-\frac{(\mu_{lim}-\mu_0)}{1.086}}]. \tag{4}$$

Here, $(\mu_{lim} - \mu_0)/1.086$ is the number of scale lengths above the limiting isophote μ_{lim}. If we substitute for m_T and assume the face-on case $b/a = 1$,

$$\log r_d = 0.2[\mu_0 - 2.5\log 2\pi - m_{lim} - 2.5\log[1 - (1 + \frac{(\mu_{lim} - \mu_0)}{1.086})e^{-\frac{(\mu_{lim}-\mu_0)}{1.086}}]. \tag{5}$$

We consider that we have completion brighter than $m_{lim} = 14.5^m$. Our fundamental reference is the Uppsala General Catalogue of Galaxies (Nilson 1973). According to Cornell et al. (1987), this catalog measures diameters to $25.4^m \pm 0.7$ at B and according to van der Kruit (1987) it measures diameters to $26.0^m \pm 0.7$ at B. In the following, we assume there is completion to $\mu_{lim}^B = 25.5^m$. With these assumptions for m_{lim} and μ_{lim}, Eq. (5) provides the relation between r_d and μ_0 plotted as the lower limiting curve in Fig. 1. The upper left limiting curve is imposed by the requirement that galaxies have diameters larger than 1 arcmin at the limiting isophote. In this case,

$$r_d(\mu_{lim} - \mu_0)/1.086 > 30'' \tag{6}$$

that is, the scale length times the number of scale lengths above the limiting isophote must exceed a radius of $30''$.

The galaxies of the complete sample seem already to fall into two zones in each of the color panels of Fig. 1. As one progresses from B, through R and I, to K', the two zones become more separated. The higher surface brightness galaxies tend to be redder so the differences between high and low surface brightness objects are accentuated with observations toward the infrared.

2.2 Inclination corrections

Inclination effects can be confusing at optical bands because surface brightness pathlength and obscuration variables play off against each other. Happily, at K' obscuration is negligible and it can be anticipated that projection effects on surface brightness are simply described by geometric considerations. It is expected that the central surface brightnesses of galaxies viewed face-on can be described by

$$\mu_0^{\lambda,i} = \mu_0^{\lambda} - 2.5C^{\lambda}\log(b/a) \tag{7}$$

Here, the coefficient C ranges from 0 for an opaque system to 1 for a transparent system. The superscript i means that an inclination correction has been applied. It can be anticipated that $C^{K'} \sim 1$ at K' and C^{λ} is progressively smaller as one goes toward shorter wavelengths. In transparent systems the geometric effect of longer line-of-sight pathlengths in edge-on cases augments surface brightnesses, but if the systems are not transparent the geometric augmentation is off-set by the increased obscuration in edge-on cases.

In fact, if one distinguishes between edge-on and face-on galaxies in Fig. 1 (triangles and circles, respectively), there is an immediately evident separation between the two inclination groups on the K' plot that weakens at I and R and is almost washed out at B. It is exactly this effect that is anticipated by the formulation of Eq. (7). Estimates of C^{λ} can be derived by looking for the best agreement between edge-on and face-on galaxies in the various passbands. Given the apparent separation of galaxies into two surface brightness zones, we split the sample at $\mu_0^{K'} = 17.5$ and, moreover, consider only the 62 galaxies of the complete sample. For the high and low surface brightness sub-samples separately, we then varied C^{λ} to find minima in the dispersion of central surface brightnesses. Figure 2 illustrates the variations in rms dispersion with the choice of the parameter C, for the high surface brightness sub-sample in panel a and for the low surface brightness sub-sample in panel b. The variation of C^{λ} behaves as expected for the 39 galaxies in the high surface brightness sub-sample (38 at K'). There is a minimum dispersion at K' with $C^{K'} = 1$ corresponding to the transparent model. Progressively toward shorter wavelengths, dispersion minima occur at $C^I = 0.61$, $C^R = 0.52$, and $C^B = 0.23$. At minimum, the rms dispersions are $\sim 0.53^m$ at R and I and $\sim 0.58^m$ at B and K'. For comparison, Valentijn (1990) found $C^B \sim 0.2$ for S*b*-S*c* types and Peletier & Willner (1992) found C near the transparent regime at H-band.

If the same test is applied to the 23 galaxies of the low surface brightness sub-sample (22 at K'), the results are more uncertain but consistent with the proposition that these

systems are transparent. It is seen in Fig. 2*b* that the rms dispersion is minimized with C^λ in the range 0.64-0.78, with no systematic dependence on λ. Since C^λ does not increase with increasing λ we conclude that obscuration is not a factor for this sub-sample. The deviation from $C = 1$ is taken to be a statistical aberration. Almost certainly, $C^{K'}$ should equal unity and the measured minimum is most deviant from unity in this case. We accept that $C^\lambda = 1$ at all passbands for the low surface brightness sub-sample. Dispersions about the mean surface brightnesses are 0.5^m to 0.7^m but these values may be affected by incompletion on the low surface brightness side. Surface brightness means and dispersions are recorded for the various subsamples and passbands in Table 1.

Figure 3 is the equivalent of Fig. 1 but now with the inclination adjustments of Eq. (7) applied. In this new figure, the high surface brightness (HSB) galaxies are distinguished as the filled symbols and the low surface brightness (LSB) galaxies are identified by open symbols. The separation between the two groups is formally made at $\mu_0^{K',i} = 18.5^m$. In the K' panel, large symbols identify galaxies with large bulges (concentration index from Paper I $C_{82} > 5$). It is seen that the HSB and LSB domains are each restricted in surface brightness and extended in scale length. There are histograms of the surface brightness distributions shown in Figure 4. The one HSB system, as defined at K', that overlaps with the LSB sample at B, R, I is the anomalous galaxy NGC 3718 that will be discussed later.

These plots include the adjustments for inclination effects, so care is needed in one regard. In the cases of B, R, I the coefficients C^λ are different for the HSB and LSB regimes (see Table 1). The effect of the inclination corrections are to make the adjusted surface brightnesses of edge-on galaxies *fainter*: $\mu_0^{\lambda,i} \geq \mu_0^\lambda$. The larger the value of C^λ the larger the shift. In the case of the B, R, I passbands, since $C^\lambda_{LSB} > C^\lambda_{HSB}$ there is a *separation* of the high and low surface brightness groups introduced by the inclination adjustments. On the one hand, there is a reasonable basis for making the separate inclination corrections to HSB and LSB systems. On the other hand, it makes it dangerous to argue that the gap between HSB and LSB systems is real when part of the separation is introduced by these corrections. Hence, the K' material takes on a particular importance. Our tests indicate that both the HSB and LSB galaxies are in the transparent regime, so the two groups receive the same inclination treatment. Moreover, the HSB systems turn out to be redder than the LSB systems so the separation between the two kinds of galaxies is most easily distinguished in the infrared.

The color and reddening variations provide a reconciliation with the claims by Peletier & Willner (1992) that the range of observed surface brightness at B is small because of dust absorption and is more considerable at H where disks are almost transparent. If no corrections for inclination are made then the scatter is smallest at B because absorption and projection effects off-set each other. Once suitable corrections are made then the scatter is comparable in each band from B to K' for the separate HSB and LSB families. However the HSB and LSB families move apart as one progresses from the blue to the infrared since HSB types are redder than LSB types. Hence, if the separate families are not distinguished then the dispersion in surface brightnesses seems to increase as one progresses to the infrared.

Could the bimodality be an artifact of our fitting of the exponential disks since we have

not attempted bulge–disk decompositions? The large bulge systems are flagged in Fig. 3 and the bimodality is seen to remain in those without bulges. It is argued by de Jong (1996*b*) and Courteau, de Jong, & Broeils (1996) that the exponential representation of bulges is at least as justified as an $r^{1/4}$ representation, whence de Jong shows our "marking the disk" fits give an unbiased disk characterization relative to a bulge/disk decomposition, with an uncertainty of $\sim 0.2^m$. A greater potential error arises in our case because the K' photometry is cut off at smaller radii by sky noise. If there is a substantial bulge, the disk fitting range is restricted and there is a bias toward too steep a slope through inclusion of some of the bulge in the disk. Hence, the measure of $\mu_0^{K'}$ may be too bright. The concern here is whether bulge galaxies could have been moved from the gap to the HSB domain erroneously. The K' luminosity profile fits of Paper I have been reconsidered from a conservative perspective by asking how far $\mu_0^{K'}$ values could be pushed toward the gap. In fact, in several of the bulge systems it is warranted to take fainter $\mu_0^{K'}$ and larger $r_d^{K'}$. Changes from Paper I are recorded in Table 2. A couple of systems are moved into the surface brightness gap but the changes are not significant.

2.3 An environmental effect

Having identified the separate HSB and LSB families we wondered whether there was any environment difference between the two, so we looked at surface brightness properties as a function of proximity to nearest neighbor. Figure 5 shows the amazing result. In the top panel for each bandpass, the inclination adjusted central disk surface brightness is plotted against the projected distance to the nearest significant neighbor. To be 'significant', we require that the neighbor have at least 10% of the luminosity of the galaxy under consideration. For this discussion, we draw attention to the K' panels where the situation is clearest. Remarkably, all of the intermediate surface brightness systems have projected near neighbors. *For the* $\sim 2/3$ *of the sample that do not have a significant close companion the separation into HSB and LSB classes is compelling.*

The middle panels for Fig. 5 repeats the histograms of Fig. 4 but only includes the 38 of 62 galaxies (36 of 60 at K') in the complete sample with nearest significant neighbor more distant than 80 kpc in projection. Histogram means and dispersions are recorded in Table 1. The solid curve in the K' panel illustrates a completeness expectation. The histogram would have this shape if there was a uniform population of the $\mu_0^{K',i}-r_d$ domain for $0.8 < \log r_d < 1.6$ and $\mu_0^{K',i} > 17^m$. The fall-off from the peak is described by the transposition of the curve defined by Eq. (5) and illustrated in the B panel of Fig. 1. The bottom panels in Fig. 5 shows the same information for the 24 galaxies in the complete sample with a nearest significant neighbor closer than 80 kpc in projection.

For the isolated galaxies, there is a gap at K' between HSB and LSB types of 1.5^m, which contains 3 galaxies where roughly 20 might be expected. The dispersion about the separate peaks is $\sigma = 0.40$. There is an evident difference with respect to the representative completeness expectation. This remarkable figure demonstrates that the HSB-LSB bimodality is highly significant in galaxies that are relatively isolated today. These galaxies have transit

times $> 10^9$ years with another galaxy.

The sample is drawn from a cluster but one that appears to be dynamically young; so much so that in Paper I it was argued that the galaxies may be representative of a field population. The relatively isolated galaxies which display the bimodality most clearly are probably most similar to galaxies in the field. By contrast, the much more scattered distribution of surface brightnesses for the galaxies with projected neighbors is strong evidence that interactions can substantially redistribute the luminous matter in disks.

We can summarize this section with the suggestion that the disks of galaxies tend to be in either a high surface brightness state or a low surface brightness state and avoid the intermediate ground. At K', the difference between the mean central surface brightness of the disk components in each state is a full factor of 10. The evidence for bimodality is particularly strong if only relatively isolated galaxies are considered. The high surface brightness family lie sufficiently far from the completion limits on the $\mu_0 - r_d$ plots that our census of this family is probably near to complete. On the contrary, the low surface brightness family is badly intersected by the completion limits and our census of that family must be quite incomplete.

3 Back to the Literature

It has been appreciated for some time that there are departures from Freeman's law, to the extent that the acronyms LSB and HSB have become familiar coinage for low and high surface brightness systems. However it had never been proposed that there was a *discrete difference* between LSB and HSB galaxies. Rather, it was supposed that there was a continuum of surface brightness properties (cf, McGaugh 1996; de Jong 1996*a*) and the designations LSB and HSB described objects on either side of an ill-defined dividing line (Davies et al. 1988*a*; McGaugh & Bothun 1994; de Blok, van der Hulst, & Bothun 1995). See McGaugh (1996) for a more elaborate catagorization.

In retrospect, astronomers have long been able to distinguish LSB from HSB galaxies on a qualitative basis. Figure 6 illustrates the correlation between surface brightness class and morphological type designations. With overwhelming coincidence, galaxies typed S0–S*c* are classed HSB and galaxies typed S*cd*–I*m* are classed LSB. The few exceptions tend to be rather anomalous and hard to define morphologically. The HSB/LSB separation at $\mu_0^{K',i} = 18.5$ takes the S0 galaxy NGC 4117 to the LSB class but this limit is subjective and could be revised. Evidently, the density of the disk has a distinct signature in the appearance of a galaxy. For one thing, the HSB systems may saturate at the centers on photographic images while the LSB systems do not. There must also be manifestations in the organization of spiral structure.

Our claim of bimodality is consistent with the study by van der Kruit (1987). His sample was somewhat smaller, with distance effects, and was based on J-band photographic material with quoted uncertainties in μ_0 of $\pm 0.3^m$. He saw enough of a difference between early and late types that he fit separate distributions to the two, but he did not draw attention to

these separations or make any suggestion that the two types were distinct. Van der Kruit made inclination adjustments on the assumption that the disks are transparent which closes the gap in μ_0 between the HSB and LSB families. Consider the B-band panel of our Fig. 5. If we assumed HSB galaxies are transparent at B then the HSB sub-sample would shift to lower surface brightnesses (more positive values) by 0.6^m in the mean. The LSB sub-sample remains where it is because it was already assumed that these galaxies are transparent. Hence, the two sub-samples would begin to merge. The mean for the HSB part would be $\sim 21.2^m$, not so different from van der Kruit's $\sim 21.5^m$ for S0–S*c*II (translating from J to B) and Freeman's (1970) 21.65^m for a blend of mostly HSB and a few LSB objects.

De Jong (1996*a*) presents a similar plot to our Fig. 6 with his Fig. 3. It can be seen, on the one hand, that our results are consistent with his and, on the other hand, that his sample of mostly earlier types would not convincingly reveal bimodality.

If we are seriously proposing a distinct separation of disk types into two families, then it is an appropriate moment to try to understand the relationship between these families and the kinds of galaxies that have been revealed by other surveys. In terms of luminosity–surface brightness–scale length properties it might be argued that there are as many as *six* families of galaxy types.

Type 1: giant boxy ellipticals. Galaxies of this class do not have significant disks and are not well described by the exponential luminosity-radius description. If exponential curves were force-fit in such cases, presumably these systems would be given μ_0 values at least as bright or brighter than HSB disks and comparable scale lengths. There are no such galaxies in our sample.

Type 2: high surface brightness disks. Normal spiral and S0 galaxies, the majority of our complete sample, are of the HSB type. It can be debated if 'disky' ellipticals belong in this group or with type 1.

Type 3: low surface brightness disks. Galaxies typed S*cd* to Irregular are of this LSB class, which constitutes a third of our complete sample and a half of our overall sample. The examples we know about are inevitably HI-rich. Our study does not explore the full domain of this class at faint μ_0 and low r_d.

Type 4: dwarf spheroidals. Galaxies of this type are known in the Local Group and related objects are found in abundance in such clusters as Virgo (Binggeli et al. 1984; Impey et al. 1988) and Fornax (Ferguson & Sandage 1988; Davies et al. 1988*a*; Irwin et al. 1990). The vaste majority of these systems are HI-poor. The location of this class in the $\mu_0 - r_d$ parameter space is shown in Figure 7 with the superposition of the Fornax Cluster samples of Davies et al. (1988*a*) and Irwin et al. (1990). The domain of these dwarfs is essentially entirely below our completion limit. Galaxies of types 3 and 4 must overlap in surface brightness and scale length properties and the relationship between the two groups remains to be clarified. It has been argued (Wirth & Gallagher 1984; Kormendy 1985) that dwarf spheroidals are a distinct family from large ellipticals.

Type 5: compact dwarfs. Blue and red compact dwarfs are known to exist (Zwicky 1964). The best example of a blue compact in our sample is PGC 37045 = 1148+48 = Markarian 1460. UGC 6805 may be a reasonable example of a red compact. These two

objects are fainter than our completion limit. There is still a very poor inventory of these kinds of galaxies. Red compacts may be related to giant ellipticals and blue compacts may be related to dwarf irregulars.

Type 6: large low surface brightness galaxies. Malin 1 (Bothun et al. 1987) is an extreme example of what seems yet to be a rare class of galaxies. Other examples have been reported by Davies, Phillipps, & Disney (1988*b*) and Sprayberry et al. (1995) and representatives of these objects have been located in Fig. 7. Galaxies of this class can have extreme properties because of low values of μ_0 and large values of r_d. The objects known to date are distinguishable from galaxies of type 3 because they are relatively *red* and have *prominent bulges*. Both types 3 and 6 contain HI. It is possible that we have one galaxy of this type in our sample, albeit not so extreme. NGC 3718 is quite anomalous in comparison with the rest of our objects. It has by far the largest exponential scale length in all passbands and has a relatively low disk central surface brightness. It is red and has a big bulge which causes it to be classified S*a* but the galaxy could be considered too pathological to be fit into the Hubble sequence. Schwarz (1985) has shown that this otherwise relatively isolated galaxy could be interacting with NGC 3729. It has not been suggested in other cases that the large low surface brightness class are involved in interactions.

In summary of this section, galaxies with distinctive properties inhabit distinctive parts of the $\mu_0 - r_d$ diagram. In particular, galaxies we think of as 'normal' disk systems are reasonably *isolated* from other types in this parameter space. These normal galaxies can be quantitatively specified by their μ_0, r_d properties. We should ask how this segregation of properties has occurred.

4 A Core Surface Brightness – Luminosity Relation

This section stands a bit apart. The disk component can get lost at the centers of some galaxies that have large bulges. In Paper I, we tabulated for each galaxy the surface brightness within an ellipse with a major axis radius of $4''$ and a minor axis radius in proportion to the inclination of the galaxy. At the distance of Ursa Major, $4'' = 300$ pc. This parameter that we call μ_4 is a metric surface brightness, a measure of the density of light at the centers of all our galaxies. It is the cummulation of the light of disks and of any bulge. Active nuclei, and possibly bars, will contribute to μ_4. At K', the parameter should not be strongly affected by obscuration.

Tight correlations are seen in Figure 8 which shows all the available data at K' band. In the top panel, there is the relationship between the μ_4^i parameter and the disk central surface brightness, μ_0^i, where the superscript indicates a correction for inclination has been made. This inclination correction is applied to the disk component only; ie, the flux from the bulge contribution to μ_4 is not modified with inclination. The two parameters, μ_0^i and μ_4^i, scatter about the 45 degree equality line if there is no bulge component but $\mu_4^i < \mu_0^i$ if there is a bulge component in addition to the disk component. Only types earlier or equal to S*ab* among the HSB sub-sample have significant bulge components. In panels *b* and *c*, the K'

magnitude is plotted against the μ_4^i core surface brightness parameter and tight correlations are found. The same data are shown in the two panels but in *b* the types S*ab* and earlier are emphasized with big symbols and in *c* the types S*b* and later are emphasized with big symbols. The correlations are particularly tight with these separations by type.

These plots are a diversion from our main theme but it is worthwhile to remember that, while the disk central surface brightnesses of HSB galaxies may have a small scatter, the disk-plus-bulge (plus possible active nucleus) central surface brightnesses display a wide range. In our small sample, there are separate strong correlations between μ_4^i and $M_{K'}$ for types S0–S*ab* and S*b*–I*m*.

5 Luminosity Functions

A convenient description of the luminosity function of galaxies is provided by the Schechter (1976) formulation. However, there is growing evidence that this two-parameter curve is too simple. Samples that are fit only to $M_B \lesssim -16^m$ are adequately described with the Schechter parameter $\alpha \simeq -1.0$ (Davis & Huchra 1982; Tully 1988; Loveday et al. 1992; Marzke et al. 1994) which is the case if there are equal numbers in equal logarithmic bins at faint luminosities. However, there have been claims that the luminosity function turns up, possibly dramatically, at the faint end (Sandage et al. 1985; Driver et al. 1994; Marzke et al. 1994). In other words, the luminosity function for all galaxies combined may have a concave shape that the Schechter formulation will not accommodate.

It is interesting to see the separate contributions to the total luminosity function according to the HSB and LSB catagories that have been identified. Figure 9 shows the luminosity functions of the separate HSB and LSB components and the sum of all types. Overall, the luminosity function is rather flat to the completion limit of $M_B = -16.5^m$. The separate components have very different forms. The HSB component *cuts off above the completion limit* while the LSB component is rising sharply at the completion limit.

This result is not surprising given the strong correlation between the surface brightness classes and morphological types, as shown in Fig. 6. Sandage, Binggeli, & Tammann (1985) have demonstrated the differences in luminosity functions between morphological types. See also Binggeli, Sandage, & Tammann (1988) for a review, and Marzke et al. (1994). The Binggeli et al. review recalls the historical debate over the bell-shaped function found by Hubble (1936) versus the faint-end exponential shape advocated by Zwicky (1942). It has been appreciated that Hubble was drawing upon a sample dominated by high surface brightness objects while Zwicky was impressed that low surface brightness, faint galaxies did exist but were strongly selected against. There are some basic points of agreement. Binggeli et al. (1988) find bell-shaped luminosity functions for types E–S*c*, as we do for the HSB family, and as Hubble found for samples dominated by HSB galaxies. Binggeli et al. and Marzke et al. (1994) find luminosity functions to be steeply increasing at the faint end for irregular or dwarf spheroidal systems, as we find for the LSB family and as Zwicky anticipated.

The HSB–LSB distinction does put a new twist on the debate. It was not clear before why

one should be impressed by the decomposition of the luminosity function by type carried out by Binggeli et al. Let us restrict our considerations to either the HI-rich disk systems or the HI-poor ellipsoidal systems separately. If there is a continuum of properties along one of these branches then the type decomposition may just be providing an alternative description of the Hubble sequence rather than telling us something fundamental about galaxy formation. For example, suppose the sequence from Sa to Im is basically a continuous mass sequence. More massive galaxies are more organized, have bigger bulge components, get an earlier type classification, and are more luminous. The least massive, less luminous galaxies are too small to maintain spiral structure and have a late type classification. Naturally then, there would be differences in the luminosity functions of the different types and earlier types will have cut-offs at the faint end. The luminosity function differences between types might just be telling us about thresholds for the maintenance of spiral structure or the formation of bulges: issues to do with resonances or disk instabilities, perhaps. The ensemble luminosity function might be viewed as providing a more global constraint on the mass spectrum and galaxy formation.

The HSB–LSB dichotomy provides a better understanding of the origins of the historic debate and enhances the interest in the separation of luminosity functions by type. If there really were a continuum of surface brightness properties among disk systems then the extreme bias of early and even modern surveys in favor of E–Sc types at the expense of Sd–Im types is hard to understand, the 'visibility' arguments of Disney & Phillipps (1983) not withstanding. The situation makes more sense if there is a distinct gap in the detectability of the early and late types, as follows from what we are finding. Moreover, the gap has to be explained. The step from Sc to Sd may involve a discontinuity in formation processes. For example, what if there is a step in mass-to-light ratio between the Sc and Sd types, a possibility discussed in the next section. Then the ensemble luminosity function would not be a simple reflection of the more fundamental mass function. A kink in the ensemble luminosity function between the domains of HSB and LSB dominance might be a signature of a break between different ways that disks form.

6 Luminosity – Line Width Relations

Although the possibility of surface brightness bimodality has come as a surprise, part of the original motivation for our study was to understand why galaxies can lie together on a luminosity–HI profile line width plot (Tully & Fisher 1977) yet be quite removed from each other on a surface brightness–scale length plot. The luminosity–line width relations are seen in Figure 10 for the fraction of our sample that satisfies our type, inclination, and HI profile quality criteria (34 galaxies). The HSB galaxies are distinguished by filled symbols; the LSB galaxies, by open symbols.

In all the passbands, it can be seen that there is a $2^m - 3^m$ domain of overlap between HSB and LSB galaxies and that there is no significant difference of each type from the mean correlations. The HSB systems are redder than the LSB systems so the HSB types do

progressively brighten relative to the LSB's as one steps toward the infrared. The galaxies in the overlap region are given box symbols so they can be tracked in the next plot, Figure 11. This figure is a repetition of Fig. 3 except now the galaxies given box symbols in Fig. 10 are identified with identical symbols here. These figures illustrate the point made in the previous paragraph. Galaxies that are mixed together in luminosity–line width diagrams separate to the distinct HSB and LSB zones on the $\mu_0 - r_d$ diagrams.

Three specific HSB–LSB pairs are illustrated in Figure 12. Each of these pairs lies close together on the luminosity-line width diagrams. See the objects labeled 1,2,3 in Figs. 10 and 11. The I-band inclination-adjusted surface brightnesses are shown in Fig. 12 and the distinct differences between the HSB and LSB families are evident.

The HSB-LSB overlap in Fig. 10 is part of the mystery of the tightness of luminosity–line width relations. The coincidence between LSB and HSB systems has been noted by Sprayberry et al. (1995) and Zwaan et al. (1995). Zwaan et al. make the following point if galaxies are built homologously. Compare systems with the same luminosity L and maximum rotation velocity V_{max}^{obs} but different μ_0, r_d. Then the indicative mass, $M \propto (V_{max}^{obs})^2 r_d$, is greater for the LSB galaxy with large r_d than the HSB galaxy with small r_d, though the luminosities are the same. That is, $(M/L)_{LSB} > (M/L)_{HSB}$. This argument is in line with other evidence that late-type galaxies have larger mass-to-light ratios than early-types (Carignan & Freeman 1988; Persic & Salucci 1988).

If the velocity field is responding to just the matter distributed in an exponential disk then the velocity maximum induced by this disk, V_{max}^{disk}, will occur at $2.1 r_d$ (Freeman 1970). With this consideration, we can generalize that there are three possible cases: (i) if the potential within a few r_d is dominated by mass in an exponential disk then the observed V_{max}^{obs} should occur at $r \sim 2.1 r_d$, (ii) if the potential is dominated by the halo V_{max}^{obs} will probably occur at $r > 2.1 r_d$, since the halo is expected to be more extended than the light, and modeling will probably give $V_{max}^{disk} \ll V_{max}^{obs}$, and (iii) if in addition to the self-gravitating exponential disk there is a central bulge then V_{max}^{obs} should be pulled inward to occur at $r < 2.1 r_d$.

We can look at the information about velocity fields in the literature. The HSB–LSB pair NGC 2403–UGC 128 was studied by de Blok & McGaugh (1996) because they share the same V_{max}^{obs} and L. The HSB object NGC 2403 has an exponential disk scale length about a third that of the LSB object UGC 128. The luminosity is sufficiently concentrated in the HSB case that the stellar mass that can be associated with the light is enough to produce the observed velocities. Such is not the situation with the LSB case. The resolution in the case of UGC 128 is not fully satisfactory (beam $\sim 2 r_d$). Verheijen (1997) has Westerbork HI synthesis maps of all the galaxies, both HSB and LSB, in the overlap region of $-17^m > M_B > -19^m$ of the Ursa Major sample. Figure 13 provides a preview of a small bit of the HI information available to us. Velocity–radius contour maps are shown for the triplet of galaxies tracked in Figs. 10 and 11.

The three galaxies used in this figure were chosen as representatives of the three generalized cases outlined two paragraphs above. We will try to make the case that NGC 3949 is an example of a self-gravitating exponential disk system without a substantial bulge. This galaxy is in the HSB family. It is offered as an example of case (i) above and will be referred

to as the "exponential HSB" class. UGC 6973 has an HSB disk and, additionally, has a significant central excess of light. It is offered as an example of case (iii), the "exponential HSB plus bulge" class. NGC 3917 is drawn from the LSB family. It will be shown that the disks of such galaxies do not make an important dynamical contribution. This object is an example of case (ii), the "LSB" class.

The bottom panels of Fig. 13 demonstrate decompositions of the rotation curves according to the contributions associated with the stellar component, assuming $M/L_{K'} = 0.4 M_\odot/L_\odot$, the interstellar gas component (negligible in all these examples), and what is left over, hence attributed to a dark halo. The choice $M/L_{K'} = 0.4 M_\odot/L_\odot$ was made to give a 'maximum disk' fit (van Albada & Sancisi 1986) of the velocities associated with the luminous matter to the observed inner rotation velocities for UGC 6973 and NGC 3949, the two HSB examples. There was no attempt to make a bulge-disk decomposition. For the LSB NGC 3917, the same choice of M/L fails by a wide margin to explain the observed rotation. The disk contribution could be raised with an increased $M/L_{K'}$ but not sufficiently for it to become dominant. If anything, it might be expected that M/L values are lower for LSB systems compared with HSB types, not higher. The idea that there is a dynamical difference between HSB and LSB types is revisited in the next section. The photometric gap appears to have a dynamical correspondence.

7 Discussion

A discreteness between 'normal' and 'dwarf' galaxies was suggested by Dekel & Silk (1986) based on a theoretical idea, though the idea was motivated by observations. They argued for a potential well *threshold*: small galaxies loose much of their gas when an early burst of star formation leads to supernova driven winds that exceed the escape velocity, while large galaxies retain the gas.

The concept could explain the distinction between LSB and HSB conditions and the apparent augmentation in M/L with LSB types. It may be a problem for the theory that there are examples of the LSB class within our small sample that have rotation velocities as high as $V_{max}^{obs} \sim 150$ km s^{-1}, since Dekel and Silk predict there is substantial mass lose only if virial velocities are $\lesssim 100$ km s^{-1}. Perhaps that stretch can be accommodated. However, we have a more fundamental concern.

It is not evident how the Dekel–Silk model fits with the observation that HSB and LSB systems of a given maximum rotation value have the same luminosity. Their 'dwarfs' loose a large fraction of the gas that could create stars and luminosity. Alternatively, these observations could be satisfied if two conditions are met: (i) *the maximum velocity of a galaxy is set by the dark halo*, and (ii) *there is a fixed initial fraction of the protogalaxy in matter that can form stars and this matter is largely conserved.* This latter condition is quite at odds with the Dekel–Silk proposition, although remember that we need only be concerned with the domain $-19^m < M_B < -17^m$ where HSB and LSB types overlap. The Dekel–Silk mechanism could kick in at a fainter magnitude.

If our two rules are met then the observations of Figs. 10 and 11 can be explained since a predictable number of stars are formed in a given halo, though the concentration may vary. We need a *different* mechanism from that proposed by Dekel and Silk, one that creates the discrete HSB and LSB classes while *preserving* the dissipational mass content.

Mestel (1963) pointed out that self-gravitating disks would find their ways to specific radial configurations since there are radial forces in disks that are not experienced if there is spherical symmetry. Mestel anticipated that one stable radial gradient results in a flat rotation curve. Gunn (1982) has shown that a flat rotation curve due to a dynamically important disk embedded in an isothermal halo implies an exponential mass distribution for the disk. Ryden & Gunn (1987) get flat rotation curves with galaxy formation in a cold dark matter scenario but the halos are dominant. Ryden (1988) could find an inner regime where the dissipational material is dynamically dominant in cases with large initial fluctuation amplitudes which become large galaxies. These models do not entertain possible transfer of angular momentum between successive collapsing shells during formation.

Our proposition is that the HSB and LSB modes correspond to two alternative radially stable configurations. To understand the two possibilities, let us consider the large and small extremes, then the intermediate cases. The small extreme may be the simplest. Suppose that the dissipational component has sufficient angular momentum that it reaches rotational equilibrium at densities that still leave the halo dominant. If small galaxies that have avoided merging are the progeny of small amplitude ($\sim 1\sigma$) initial fluctuations then it is reasonable that they formed late, hence with relatively high specific angular momentum (Efstathiou & Jones 1979)

One of Mestel's (1963) stable configurations involves self-gravitating diffuse disks but there is evidence from disk–halo decompositions that the diffuse LSB disks are *not* self-gravitating (Fig. 13, NGC 3917, and de Blok & McGaugh 1996). The dark matter halos contribute substantially at all radii. If this quasi-spherical system collapsed conserving angular momentum in radial shells then it ends up in the stable configuration described by Ryden and Gunn.

The luminous galaxies find their way to become disk dominated at their centers. Somehow we end up with the disk–halo 'conspiracy' of flat rotation (van Albada & Sancisi 1986). There have been a lot of experiments with N-body simulations in the framework of the cold dark matter model and there is general agreement with the observed rotation properties of galaxies (cf, Blumenthal et al. 1986; Navarro, Frenk, & White 1996). There are systematics that make the 'conspiracy' less than perfect, with some initial decline with radius in concentrated, luminous systems (Casertano & van Gorkom 1991). The central densities of the disks remarkably conform to Freeman's law. Galaxies know the law. If there is too much dissipational material in the cores to abide the law then a bulge is formed. The 'conspiracy' co-ops this third component.

Our qualitative interpretation of events is that the galaxies have settled into a mandated stable radial configuration, in the spirit of the Mestel argument but with the revision required due to the lurking dark halo. The formation process presumably involved a considerable transfer of angular momentum outward to the halo. Such a process would seem to be a

natural consequence of hierarchical merging where blobs come together in non-axisymmetric ways, and is seen in N-body simulations (Barnes & Efstathiou 1987) and collision simulations with gas (Barnes & Hernquist 1991). The differences in the surface brightness distributions for galaxies with, and without, close neighbors, seen in Fig. 5, provides strong evidence that interactions can reorganize the luminous matter in galaxies. Even without such jostling, the Ryden (1988) models show that more massive systems (with parts that form earlier with less angular momentum) have more significant dissipationally dominant cores. The dissipational collapse of disks was discussed by Fall & Efstathiou (1980) and we can mention the contribution by Shaya & Tully (1984).

Two stable radial configurations have been identified. In massive systems with a significant component of low angular momentum material, the dissipational matter will collapse to form a dynamically important disk that rotates with a velocity tied to the requirements of the dark halo. In dwarf systems the dissipational material does not collapse enough to dominate the dark halo even near the center. Now consider the intermediate regime. The evidence from the Ursa Major Cluster sample is that *galaxies opt for one of the two aforementioned stable configurations rather than find some state in between.* There is a two to three magnitude domain between giants and dwarfs where the galaxies have a choice. It is seen from Fig. 9 that, proceeding from bright galaxies to faint, the number of HSBs drop and the number of LSBs picks up. The evolutionary path followed by a specific intermediate-size galaxy must depend either on the amount of angular momentum it acquired as a protocloud or on the degree of trauma of it's birth and during it's lifetime. Systems that retain lots of angular momentum hang up as LSB galaxies. Systems that never had much angular momentum or, probably more relevant, those that transfer angular momentum outward collapse to the HSB state.

The focus has been on the distinction between LSB and HSB families. There is the second transition between systems that are exponential disks to their cores and systems with central bulges. Both varieties have disks that obey Freeman's law. Densities do not want to exceed the mandated threshold in a rotating disk. If there is low angular momentum material that would cause an excess then it finds its way into a bulge.

What we have been presenting at first blush seems to contradict the 'universal rotation curve' idea of Persic, Salucci, & Stel (1996). How can our three discrete states be reconciled with their continuum of rotation properties as a function of total luminosity? The apparent contradiction at the state transition between bulge/no–bulge can be disregarded because Persic et al. make the disclaimer that their 'universal rotation curve' may not apply at small radii in cases of bulges. As for the state transition between HSB and LSB, it depends on how one looks at the data. In Fig. 13 it is seen that HSB and LSB systems have very distinct *metric* radial distributions because the LSB types are much more extended. However the rotation curves are only different in a subtle way if the radial scale is *normalized* by either exponential scale length or optical radius as Persic et al. do. The exponential HSB NGC 3949 reachs V_{max}^{obs} at $\sim 2.1 r_d$, located by the little arrow in the lower panel of Fig. 13. The LSB NGC 3917 reachs V_{max}^{obs} somewhat farther out than this photometric scale length located by the arrow. It will take a large sample of high quality velocity fields to confirm if the rotation

curves are continuing to rise at $\sim 2.1 r_d$ in LSB types while they tend to have peaked by this radius in HSB systems of the corresponding luminosity. Since the HSB and LSB types overlap in luminosity, it can be understood how the very small differences in normalized curves get averaged and result in a smoothly continuous 'universal rotation curve'.

It is important to recall the point made by Zwaan et al. (1995), however. The masses and M/L measures are functions of the *metric* radii. Hence, though the scale length–normalized rotation curves of an HSB–LSB pair of a given luminosity might be almost indistinguishable, still $(M/L)_{LSB} > (M/L)_{HSB}$ within the optical domains. In the case of the HSB galaxies, it was seen in Fig. 13 that model velocities V_{max}^{disk} approaching V_{max}^{obs} can be associated with the light and M/L values characteristic of star ensembles. By contrast, for LSB systems the velocities V_{max}^{disk} associated with stars and gas fall far short of V_{max}^{obs} (see also de Blok & McGaugh 1996, 1997). Qualitatively, V_{max}^{disk} is given by the relationship:

$$\frac{(V_{max}^{disk})^2}{L} \sim \frac{(M/L)}{r_d}. \tag{8}$$

In an HSB system, r_d for a given L is small and the required M/L to give $V_{max}^{disk} \sim V_{max}^{obs}$ is reasonable. In an LSB system with the same L and V_{max}^{obs}, there is a larger r_d and the required M/L to give $V_{max}^{disk} \sim V_{max}^{obs}$ is unreasonably large for a stellar system. If anything, the blue LSBs can be expected to have *lower* M/L values than redder HSBs.

Note that Persic et al. (1996) are arguing as we do that low luminosity galaxies have much more important dark halo contributions within the optical domain than is the case with high luminosity galaxies. The difference is that they see the transformation with luminosity as a continuum while we think there is a discrete transition involved. Our point-of-view receives some support from information in the literature. As in Fig. 13, disk–bulge decompositions of well-established rotation curves lead to models where *either* the disk component substantially dominates the halo interior to $\sim 2 r_d$ *or* the disk component is at best comparable to the halo at the center. We are unaware of a well established case where the disk is only modestly dominant at the center.

8 Linkage Between Photometric and Kinematic Properties

A direct linkage can be drawn between the surface brightness bimodality and a dynamical bimodality. The luminosity–line width fits given by the lines in Fig. 10 translate to relationships between rotation velocities, surface brightnesses, and scale lengths given Eq. (3) and our assumed distance to the sample of 15.5 Mpc. At K' band:

$$\log W_R^i/2 = 3.355 - 0.112 \mu_0^{K',i} + 0.561 \log r_d^{K'}. \tag{9}$$

Here, $W_R^i/2$ approximates V_{max}^{obs} and, to be precise, this relation is based on the double regression to the data in Fig. 10 rather than the single regression with errors in W_R^i that we

use for distance measurements. At the same time, the peak rotation velocity that arises out of an exponential disk is given by:

$$V_{max}^{disk} = 8.60 \times 10^4 \sqrt{10^{-0.4\mu_0^{K',i}} r_d^{K'} M/L_{K'}} \tag{10}$$

or in the logarithmic form:

$$\log V_{max}^{disk} = 4.934 - 0.2\mu_0^{K',i} + 0.5\log r_d^{K'} + 0.5\log M/L_{K'} \tag{11}$$

where V_{max}^{disk} in km s^{-1} is the peak rotation velocity at $2.1r_d$ for an exponential disk, in the units of Figs. 1, 3, and 11 at our assumed distance. The coefficient of Eq. (10) is 3.14×10^5 if the units of r_d is kpc. Combining these equations,

$$\log(V_{max}^{disk}/0.5W_R^i) = 1.579 - 0.0878\mu_0^{K',i} - 0.0610\log r_d^{K'} + 0.5\log M/L_{K'}. \tag{12}$$

Suppose a fixed value of $M/L_{K'}$ is assumed. The maximum disk fits illustrated in Fig. 13 suggest $M/L_{K'} = 0.4M_\odot/L_\odot$. Then a choice of $V_{max}^{disk}/0.5W_R^i$ translates to an almost horizontal line in Fig. 11. The solid line illustrates $V_{max}^{disk}/0.5W_R^i = 2/3$ and the dashed line illustrates $V_{max}^{disk}/0.5W_R^i = 1/3$. The lines would be exactly horizontal if the coefficient for the term in $\log r_d$ in Eq. (9) were 0.5, which would arise if $L_{K'} \sim (W_R^i)^4$. Instead the double regression of the K' panel of Fig. 10 gives $L_{K'} \sim (W_R^i)^{3.6}$. These lines make graphic the point first discussed by Aaronson, Huchra, & Mould (1979): the relation $L \sim (W_R^i)^4$ is explained if μ_0 and M/L are constants for disk galaxies and $V_{max}^{obs} \sim V_{max}^{disk}$.

Eq. (12) tells us that the bimodality in μ_0 implies a bimodality in either $V_{max}^{disk}/0.5W_R^i$ or M/L. A bimodality in M/L is unlikely since it would require that, at all bands from B to K', M/L is greater (substantially!) for LSB galaxies though these systems are known to have proportionately younger populations than HSB galaxies. It is much more probable that the bimodality is in $V_{max}^{disk}/0.5W_R^i$.

Accepting the simplifying assumption that M/L = constant (specifically, $0.4M_\odot/L_\odot$ at K'), then any location in the μ_0, r_d plane corresponds to a determinate vale of $V_{max}^{disk}/0.5W_R^i$ from Eq. (12). Figure 14 is the histogram of all such values for the isolated fraction of our sample (those with no significant neighbors within 80 kpc in projection). Except for the weak dependence on r_d identified in Eq. (12), Fig. 14 is essentially a rescaling of the middle K' panel of Fig. 5.

The rotation curve decompositions of Fig. 13 help with the interpretation of this rescaling of the bimodality phenomenon. With the HSB cases, V_{max}^{disk} is a substantial fraction of V_{max}^{obs}. Halo components contribute but the disk components are dominant inside $2r_d$. For example, with NGC 3949 the decomposition gives $V_{max}^{disk}/V_{max}^{obs} = 0.68$. By contrast, in the LSB case, NGC 3917, $V_{max}^{disk}/V_{max}^{obs} = 0.39$. It can be seen in Figs. 10 and 11 that NGC 3917 is one of the most luminous LSBs and at the high surface brightness limit of the LSB family. Yet even in this case, the dark halo potential dominates the disk at all radii. Hence the bimodal distribution in Fig. 14 can be given a dynamical interpretation. The galaxies in the peak about $V_{max}^{disk}/0.5W_R^i = 0.73$ have self-gravitating disks with rotation in response to

the luminous matter at $r \lesssim 2r_d$. The galaxies in the peak about $V_{max}^{disk}/0.5W_R^i = 0.42$ have dynamically insignificant disks in dominant dark halos. These two dynamical classes have direct correspondences with the photometric HSB and LSB classes, respectively.

A qualitative story has been presented. More detailed velocity field data are required to go further, and of course more quantitative modeling. There is the usual disclaimer that we have assumed Newtonian gravity is valid in this regime, for if not then the discussion of this section is built on a bogus premise (Milgrom 1983; Sanders 1984; Mannheim 1993). Still, the bimodal surface brightness observations have to be explained.

9 Summary

There is suggestive evidence that galaxies *avoid a region of parameter space* between high central surface brightness and low central surface brightness domains. The statistics provided by the present sample are insufficient to make the case compelling, however it will be straightforward to check our claim with larger controlled data sets. Since we are predicting a minimum between two distributions, any experimental criteria that includes both the HSB and LSB regimes should properly sample the intermediate zone. The case for bimodality of surface brightnesses is strongest for galaxies without near (< 80 kpc) neighbors.

We argue that *the luminosity function for the high surface brightness family cuts off at the faint end.* Again our results have some uncertainty because the cut-off is close to our completion boundary. It will be easy to design an experiment that goes a magnitude deeper and checks this claim.

There is the curiosity that *galaxies of a given luminosity, whether of high surface brightness or of low surface brightness, have little dispersion in HI profile width.* Yet the light of HSB and LSB galaxies is distributed so differently that it would be surprising if the rotation curves of these classes were not correspondingly different. Preliminary evidence is presented that suggests that the 'exponential HSB' class have rotation curves that peak by $\sim 2.1r_d$, as anticipated for dynamically important exponential disks, while there is evidence that the 'LSB' class have rotation curves that continue to rise beyond this radius. In the HSB types it appears that reasonable stellar M/L values produce inner rotation velocities that rise close to V_{max}^{obs}, while for LSB types velocities associated with reasonable models of the disk components fall considerably short of V_{max}^{obs}.

The dichotomy between HSB and LSB types implies to us that there are two basic control conditions: (i) maximum rotation is mandated by the dark halo, and (ii) there is a fixed fraction of precollapse dissipational material that is preserved to give the observed luminosity. The latter point is at odds with the idea that the LSB class is the result of gas loss during an early starburst phase, but is the obvious explanation of the tightness of luminosity–line width relations. The HSB and LSB types of a given luminosity would live in similar halos and have the same amount of dissipational material. However the LSB types are in rotational equilibrium in potentials dominated by the dark halos at all radii, while the HSB types have either transferred angular momentum away from much of their

gas or were born with low specific angular momentum and have secularly evolved to stable states with dynamically important disks. Though in our model HSB and LSB types of a given luminosity have the same total dissipational and dark halo masses, the HSB cases have lower *measured* M/L because the light is more confined within the dark halo; ie, a smaller fraction of the total halo is within the domain of the observed rotation curve.

While the emphasis has been on the distinction between HSB and LSB families, attention has been drawn to another transition between 'exponential HSB' and 'bulge HSB' families. Freeman's law is obeyed in both cases. Evidently disks are forbidden from rising in central density above this threshold. Low angular momentum matter that would broach this limit is shunted into a bulge. The bulges have a clear manifestation in the rotation curves. Velocities approach maximum values much closer to the centers than the radius $\sim 2.1 r_d$ characteristic of the peak for self-gravitating exponential disks. There could be said to be the maintenance of the flat rotation curve 'conspiracy'.

It is pointless to go too far with speculation in the absence of much detailed rotation curve information, but the potential importance of these results should be given attention. Only discrete radial gradients of matter are stable for disk systems since, unlike in spherical systems, a particle in orbit at a given radius feels the net gravity of mass at larger radii. Galaxies must arrange themselves into one of these discrete states. Evidently, galaxies of intermediate mass have a choice.

10 Acknowledgements

Mike Pierce, Jia-Sheng Huang, and Richard Wainscoat participated in the collection of data. We thank Renzo Sancisi, Erwin de Blok, and the referee Stacy McGaugh for helpful comments. This research has been supported by NATO Collaborative Research Grant 940271 and grants from the US National Science Foundation.

References

Aaronson, M., Huchra, J.H., & Mould, J.R. 1979, ApJ, 229, 1.

Allen, R.J., & Shu, F.H. 1979, ApJ, 227, 67.

Barnes, J.E., & Efstathiou, G. 1987, ApJ, 319, 575.

Barnes, J.E., & Hernquist, L.E. 1991, ApJ, 370, L65.

Binggeli, B., Sandage, A., & Tammann, G.A. 1988, ARAA, 26, 509.

Binggeli, B., Sandage, A., & Tarenghi, M. 1984, AJ, 89, 64.

Blumenthal, G.R., Faber, S.M., Flores, R., & Primack, J.R. 1986, ApJ, 301, 27.

Bothun, G.D., Impey, C.D., Malin, D.F., & Mould, J.R. 1987, AJ, 94, 23.

Carignan, C., & Freeman, K.C. 1988, ApJ, 332, L33.

Casertano, S., & van Gorkom, J.H. 1991, AJ, 101, 1231.

Cornell, M.E., Aaronson, M., Bothun, G.D., & Mould, J.R. 1987, ApJS, 64, 507.

Courteau, S., de Jong, R.S., & Broeils, A.H. 1996, ApJ, 457, L73.

Davies, J.I., Disney, M.J., Phillipps, S., Boyle, B.J., & Couch, W.J. 1994, MNRAS, 269, 349.

Davies, J.I., Phillipps, S., Cawson, M.G.M., Disney, M.J., & Kibblewhite, E.J. 1988*a*, MNRAS, 232, 239.

Davies, J.I., Phillipps, S., & Disney, M.J. 1988*b*, MNRAS, 231, 69P.

Davis, M. & Huchra, J.P. 1982, ApJ, 254, 437.

de Blok, W.J.G., & McGaugh, S.S. 1996, ApJ, accepted in letters.

de Blok, W.J.G., & McGaugh, S.S. 1997, MNRAS, submitted.

de Blok, W.J.G., van der Hulst, J.M., & Bothun, G.D. 1995, MNRAS, 274, 235.

de Jong, R.S. 1996*a*, AAP, 313, 45.

de Jong, R.S. 1996*b*, A&AS, 118, 557.

Dekel, A., & Silk, J. 1986, ApJ, 303, 39.

de Vaucouleurs, G. 1959, Hdb. d. Physik, 53, 311.

Disney, M.J. 1976, Nature, 263, 573.

Disney, M.J., & Phillipps, S. 1983, MNRAS, 205, 1253.

Dressler, A. 1980, ApJ, 236, 351.

Driver, S.P., Phillipps, S., Davies, J.I., Morgan, I., & Disney, M.J. 1994, MNRAS, 268, 393.

Efstathiou, G., & Jones, B.J.T. 1979, MNRAS, 186, 133.

Fall, S.M., & Efstathiou, G. 1980, MNRAS, 193, 189.

Ferguson, H.C., & Sandage, A. 1988, AJ, 96, 1520.

Fisher, J.R., & Tully, R.B. 1975, AAP, 44, 151.

Fisher, J.R., & Tully, R.B. 1981, ApJs, 47, 139.

Freeman, K.C. 1970, ApJ, 160, 811.

Gunn, J.E. 1982, in Astrophysical Cosmology, ed. H.A. Brück, G.V. Coyne, and M.S. Longair (Vatican: Pontificia Academia Scientiarum), p. 233.

Hubble, E. 1936, ApJ, 84, 158.

Impey, C.D., Bothun, G.D., & Malin, D. 1988, ApJ, 330, 634.

Impey, C.D., Sprayberry, D., Irwin, M.J., & Bothun, G.D, 1996, ApJS, 105, 209.

Irwin, M.J., Davies, J.I., Disney, M.J., & Phillipps, S. 1990, MNRAS, 245, 289.

Jura, M. 1980, ApJ, 238, 499.

Kormendy, J. 1977, ApJ, 217, 406.

Kormendy, J. 1985, ApJ, 295, 73.

Loveday, J., Peterson, B.A., Efstathiou, G., & Maddox, S.J. 1992, ApJ, 390, 338.

Mannheim, P.D. 1993, ApJ, 419, 150.

Marzke, R.O., Geller, M.J., Huchra, J.P., & Corwin, H.G. Jr. 1994, AJ, 108, 437.

McGaugh, S.S. 1996, MNRAS, 280, 337.

McGaugh, S.S., & Bothun, G.D. 1994, AJ, 107, 530.

McGaugh, S.S., Bothun, G.D., & Schombert, J.M. 1995, AJ, 110, 573.

Mestel, L. 1963, MNRAS, 126, 553.

Milgrom, M. 1983, ApJ, 270, 365.

Navarro, J.F., Frenk, C.S., & White, S.D.M. 1996, ApJ, 462, 563.

Nilson, P. 1973, Uppsala General Catalogue of Galaxies, Roy. Soc. Sci. Uppsala.

Peletier, R.F., & Willner, S.P. 1992, AJ, 103, 1761.

Persic, M., & Salucci, P. 1988, MNRAS, 234, 131.

Persic, M., Salucci, P., & Stel, F. 1996, MNRAS, 281, 27.

Ryden, B.S. 1988, ApJ, 329, 589.

Ryden, B.S., & Gunn, J.E. 1987, ApJ, 318, 15.

Sandage, A., Binggeli, B., & Tammann, G.A. 1985, AJ, 90, 1759.

Sanders, R.H. 1984, AAP, 136, L21.

Schechter, P.L. 1976, ApJ, 203, 297.

Schwartzenberg, J.M., Phillipps, S., Smith, R.M., Couch, W.J.,, & Boyle, B.J. 1995, MNRAS, 275, 121.

Schwarz, U.J. 1985, AAP, 142, 273.

Shaya, E.J., & Tully, R.B. 1984, ApJ, 281, 56.

Sprayberry, D., Bernstein, G.M., Impey, C.D., & Bothun, G.D. 1995, ApJ, 438, 72.

Sprayberry, D, Impey, C.D., Bothun, G.D., & Irwin, M.J. 1995, AJ, 109, 558.

Tully, R.B. 1988, AJ, 96, 73.

Tully, R.B., & Fisher, J.R. 1977, AAP, 54, 661.

Tully, R.B., Shaya, E.J., Pierce, M.J.,& Peebles, P.J.E. 1997, ApJs, in preparation.

Tully, R.B., Verheijen, M.A.W., Pierce, M.J., Huang, J.S., & Wainscoat, R.J. 1996, AJ, 112, 2471. (Paper I)

Valentijn, E.A. 1990, Nature, 346, 153.

van Albada, T.S., & Sancisi, R. 1986, Phil. Trans. R. Soc. Lond. A, 320, 447.

van den Bergh, S. 1959, Publ. David Dunlap Obs., II, No. 5.

van den Bergh, S. 1966, AJ, 71, 922.

van der Kruit, P.C. 1987, AAP, 173, 59.

Verheijen, M.A.W. 1997, Ph.D. Thesis, University of Groningen, in progress.

Wirth, A. & Gallagher, J.S. III 1984, ApJ, 282, 85.

Zwaan, M.A., van der Hulst, J.M., de Blok, W.J.G., & McGaugh, S.S. 1995, MNRAS, 273, L35.

Zwicky, F. 1942, Phys. Rev., 61, 489.

Zwicky, F. 1964, ApJ, 140, 1467.

Table 1: Mean Central Surface Brightnesses

Filter	C_{HSB}	N	$<\mu_0>_{HSB}$	rms	C_{LSB}	N	$<\mu_0>_{LSB}$	rms
Complete sample								
B	0.23	39	20.57	±0.57	1.00	23	22.65	±0.49
R	0.52	39	19.54	±0.52	1.00	23	21.72	±0.48
I	0.61	39	18.94	±0.54	1.00	23	21.21	±0.52
K'	1.00	38	17.11	±0.58	1.00	22	19.61	±0.67
Complete subsample of isolated galaxies								
B		24	20.60	±0.52		14	22.77	±0.46
R		24	19.50	±0.55		14	21.87	±0.41
I		24	18.94	±0.54		14	21.36	±0.46
K'		23	17.15	±0.40		13	19.85	±0.39

Table 2: Revised exponential disk fits.

		Paper I		Revised	
PGC	Filter	μ_0	r_d	μ_0	r_d
35202	K′	19.31	19.6	19.9	26
36686	K′	17.04	7.1	18.0	9
37073	K′	17.09	7.9	17.8	11
37136	K′	16.90	9.3	17.3	10
37550	B	21.91	13.1	22.26	14.5
	R	20.78	11.7	21.19	13.0
	I	20.25	11.2	20.63	12.3
	K′	18.19	7.9	18.56	8.8
37553	B	21.06	16.6	21.42	18.0
	R	20.22	17.5	20.60	19.2
	I	19.88	20.0	20.30	22.5
	K′	17.87	14.6	18.34	17.1
37618	K′	16.04	8.9	16.4	10
37719	K′	14.70	11.0	17.0	18
38068	K′	16.72	30.2	16.9	33
38392	K′	16.15	19.7	15.82	18.0
38440	K′	15.63	23.9	16.02	26.3
39237	K′	16.51	7.2	16.74	7.7
38503	K′	17.11	12.1	17.8	15
38507	K′	18.26	5.7	19.1	9
40228	K′	15.91	19.7	16.8	25

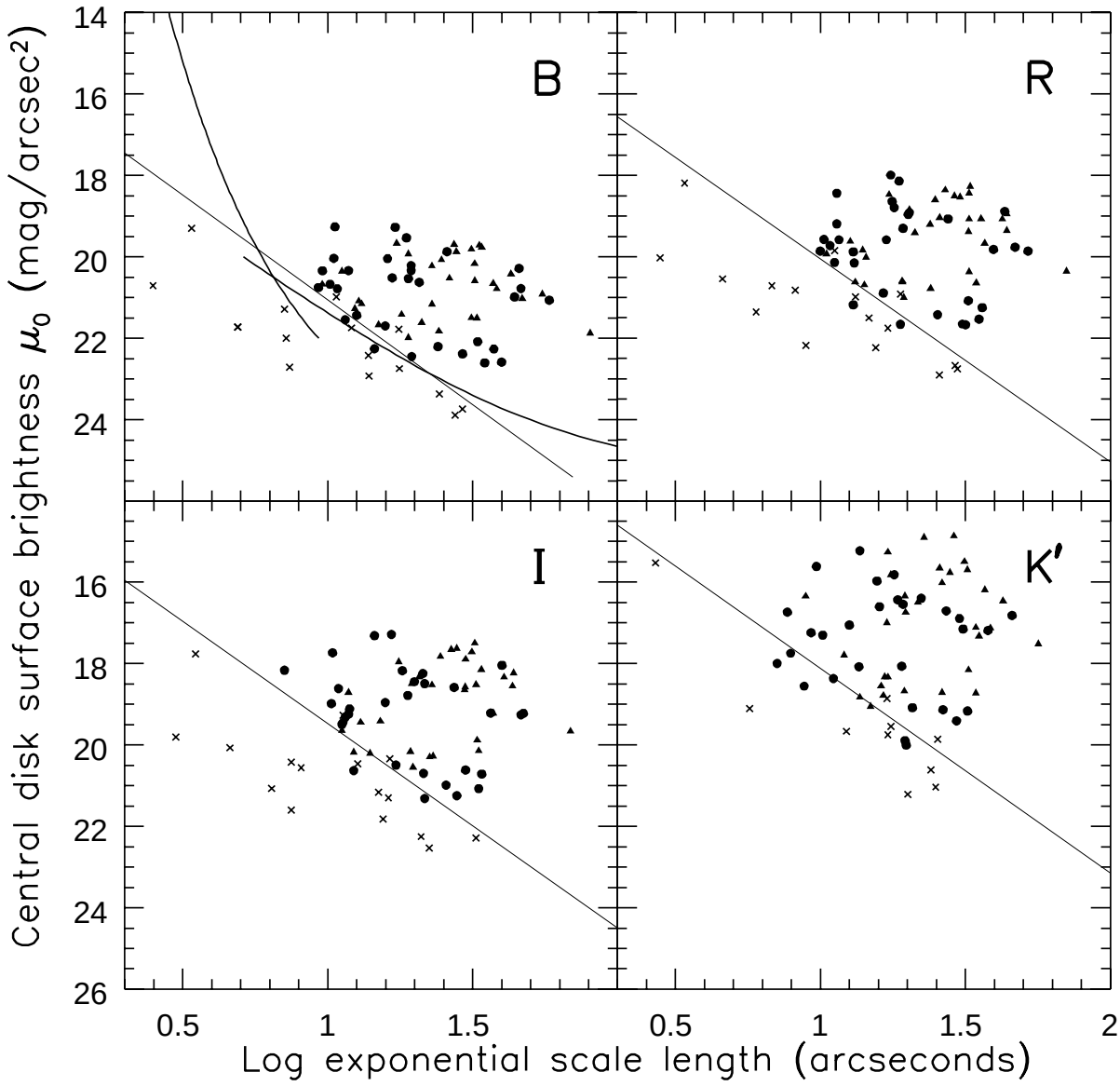

Figure 1: Central disk surface brightness μ_0 versus exponential scale length r_d. Filled symbols: 62 galaxies of the complete sample with $M_B^{b,i} < -16.5^m$; circles represent galaxies more face-on than 60° and triangles represent galaxies more edge-on than this limit. Crosses: fainter galaxies. Panels correspond to B, R, I, K' respectively. Diagonal lines at $B = 14.0^m$, $R = 13.1^m$, $I = 12.5^m$, and $K' = 11.2^m$ represent the approximate limiting magnitudes for face-on systems. For B, which is closest to the photographic band used in the sample selection, two limiting visibility curves have been superimposed. Both curves are drawn on the assumption that completion is limited by the surface brightness isophote $\mu_{lim}^B = 25.5$. Galaxies with isophotal magnitudes brighter than 14.5^m lie above the bottom curve and galaxies that are larger than 1 arcmin at the limiting isophote lie to the right of the steep curve at the left of the figure.

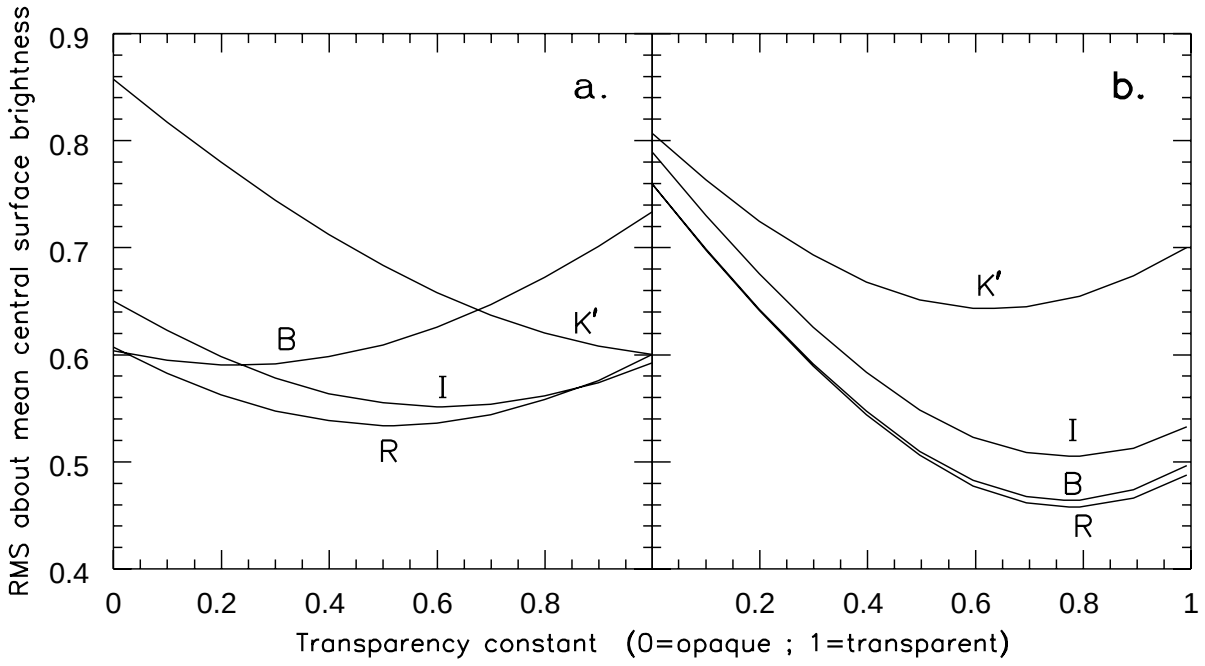

Figure 2: Dispersion about the mean central surface brightness as the transparency constant C is varied. Separate curves are given for the B, R, I, K' passbands. Panel a relates to the HSB sub-sample and panel b relates to the LSB sub-sample.

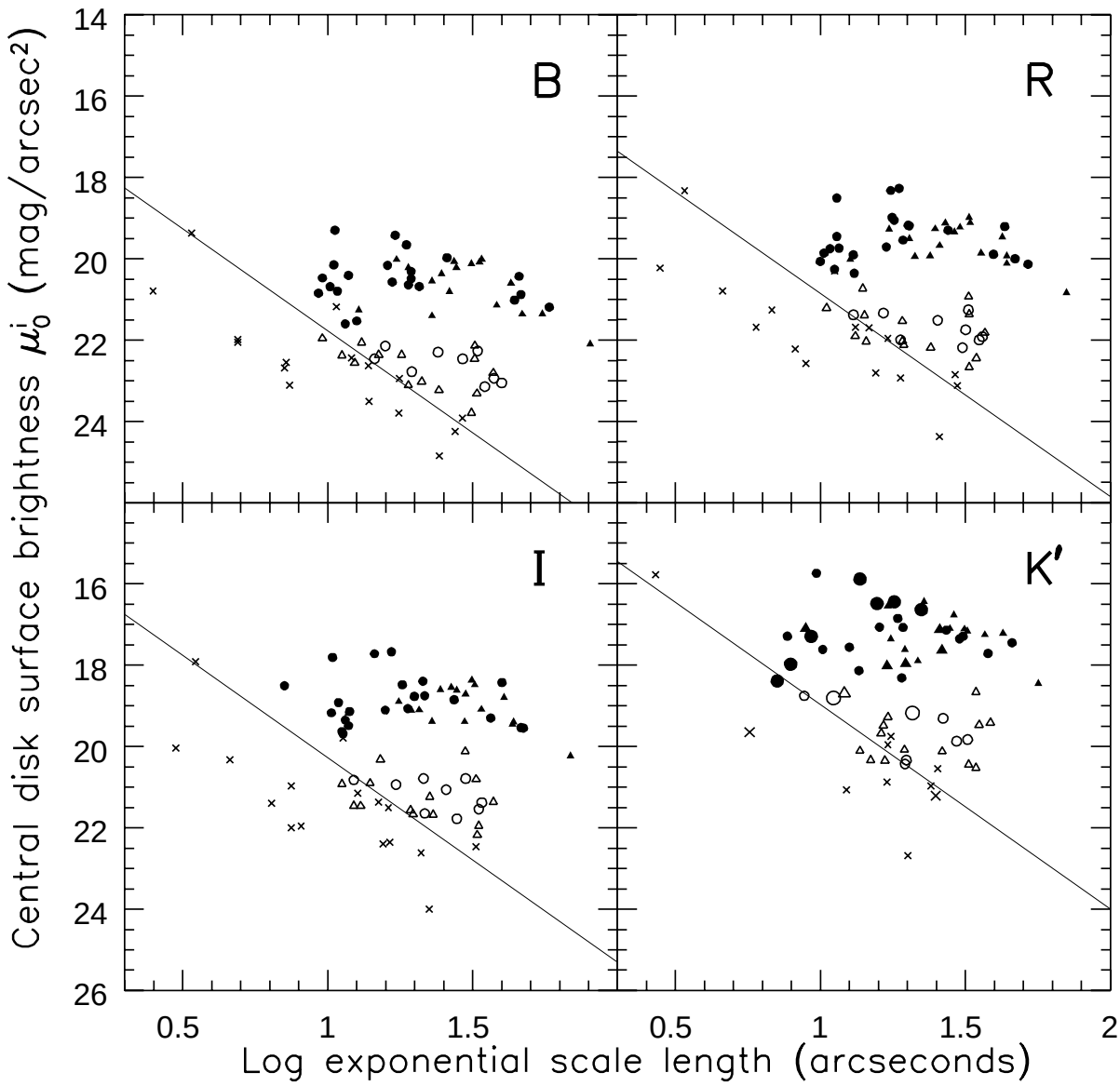

Figure 3: Inclination adjusted central disk surface brightness μ_0^i versus exponential scale length r_d. Now the complete sample is split between HSB with $\mu_0^{K',i} < 18.5$ (filled symbols), and LSB with $\mu_0^{K',i} > 18.5$ (open symbols). Again, circles represent galaxies more face-on than 60° and triangles represent galaxies that are more edge-on than 60°. The panels correspond to B, R, I, K'. Diagonal lines represent approximate limiting magnitudes, accounting for mean inclination and color transformations. Larger symbols in the K' panel identify galaxies with bulges: concentration index $C_{82} > 5$.

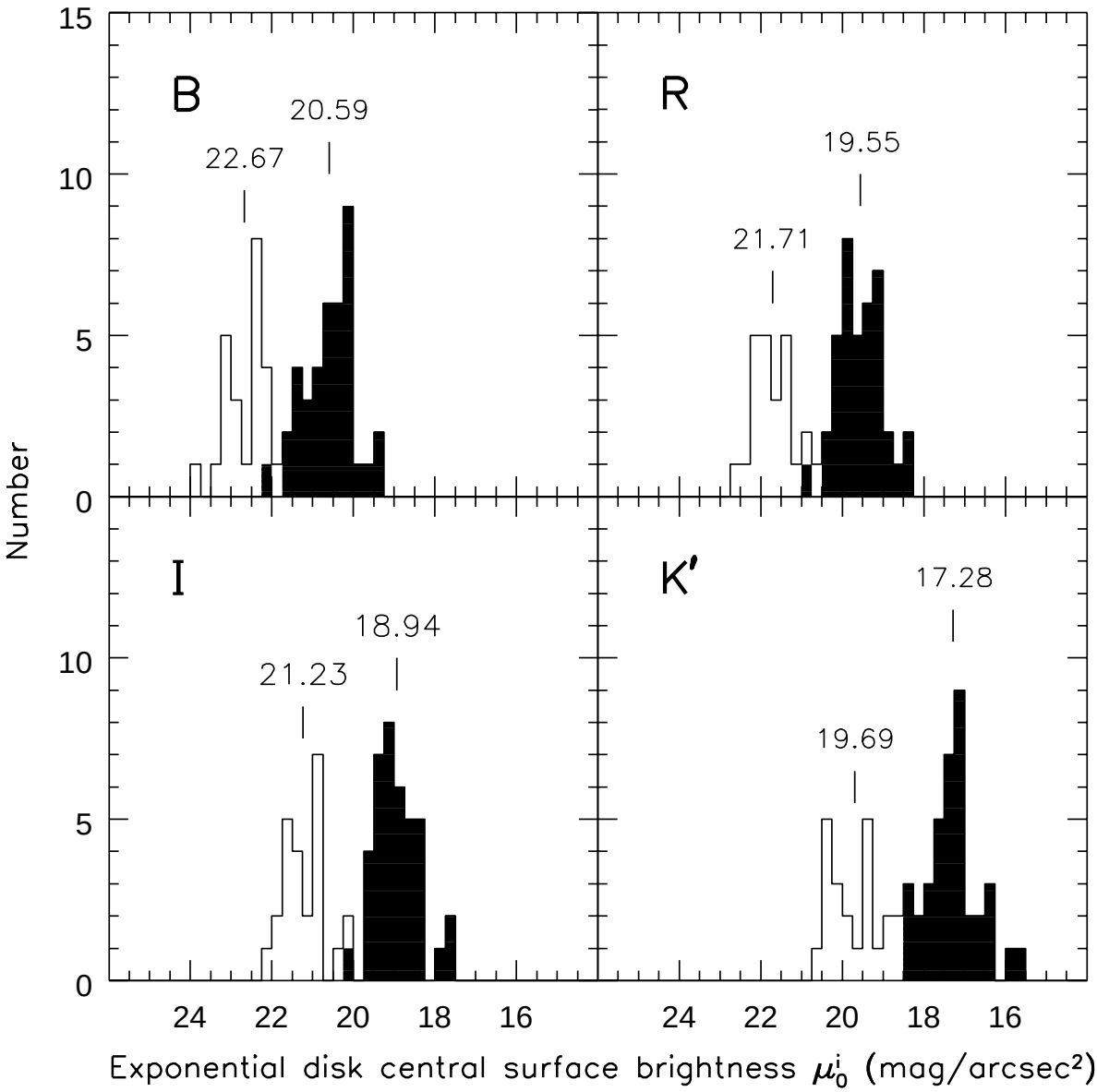

Figure 4: Histogram of inclination adjusted central disk surface brightnesses for B, R, I, K'. The HSB component of the histogram is filled. Means for the HSB and LSB components are indicated. NGC 3718 is identified as HSB at K' but lies with the LSB at B, R, I.

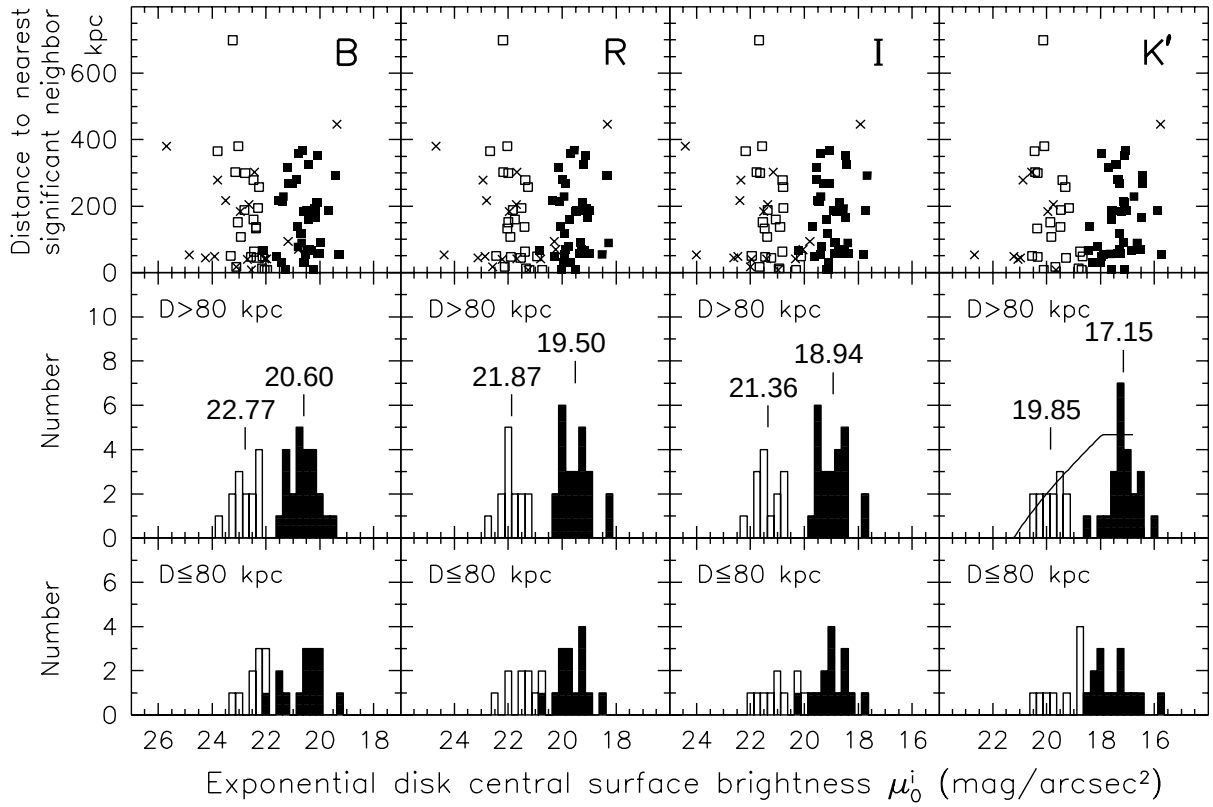

Figure 5: The effect of nearest neighbors on surface brightness. In the top panel for each of B, R, I, K', central disk surface brightnesses are plotted against the distance to the nearest neighbor with $L_{neighbor} > 0.1 L_{galaxy}$. Closed symbols: HSB; open symbols: LSB; crosses: too faint for complete sample. The bottom two panels for each passband are decompositions of the histograms of Fig. 4, complete sample only. The middle panels gives the histogram for the subset with nearest projected neighbor farther than 80 kpc and the bottom panels gives the histogram for galaxies with a projected neighbor closer than 80 kpc. The curve in the K' middle panel illustrates the completeness expectation if the surface brightness–scale length plane is uniformly populated in the interval $0.8 < \log r_d < 1.6$ and $\mu_0^{K',i} > 17^m$. The normalization of the maximum is given by the average of the three bins at the peak of the HSB distribution.

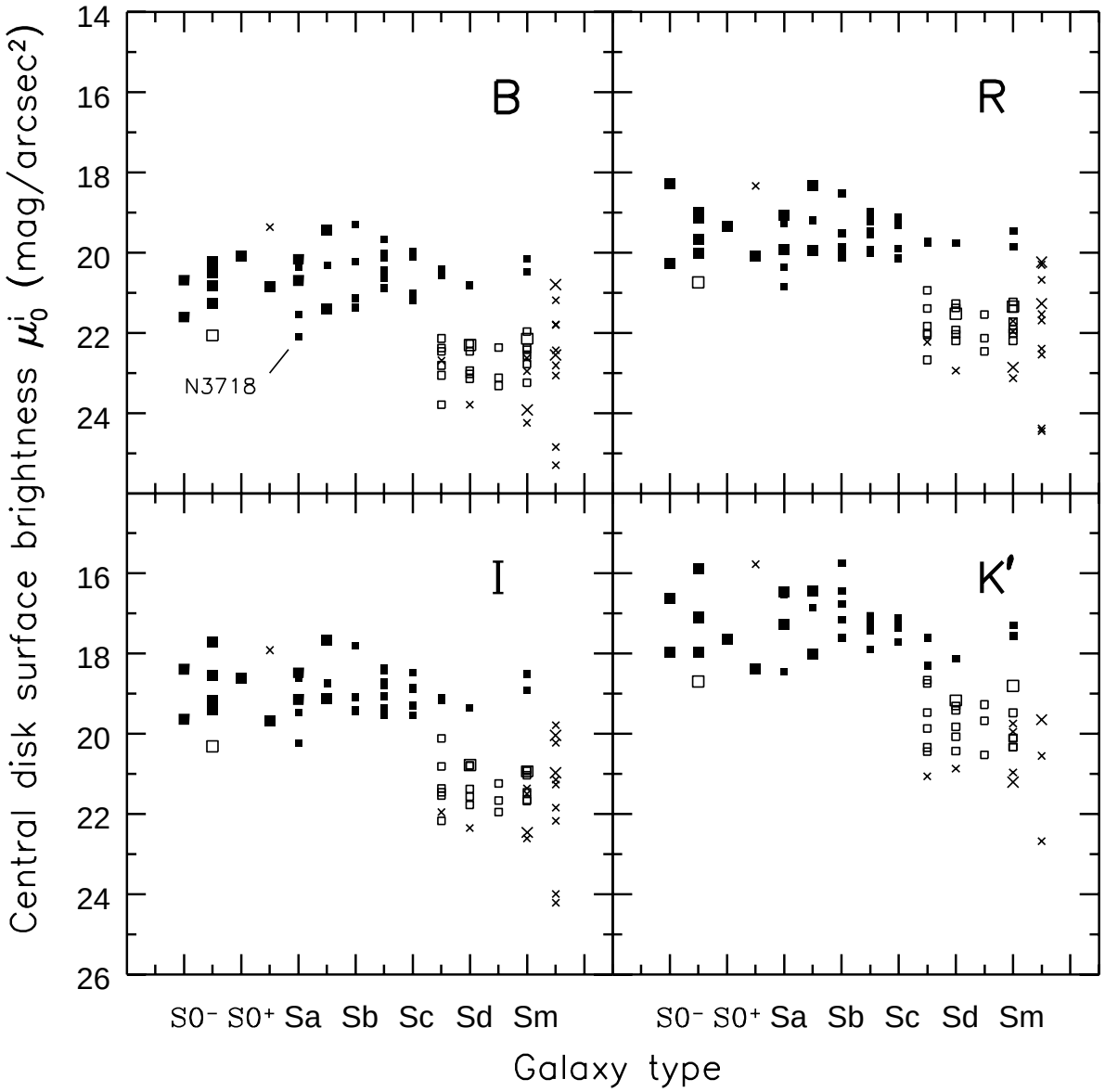

Figure 6: Correlation between surface brightness families and morphological types. Filled symbols: HSB; open symbols: LSB, crosses: fainter than complete sample limit. Large symbols denote galaxies with bulges: concentration index $C_{82} > 5$. NGC 3718 is the unusual galaxy discussed in connection with the type 6, large low surface brightness systems. The S0 galaxy identified as LSB by the delineation between surface brightness regimes at $\mu_0^{K',i} = 18.5$ is NGC 4117. Otherwise, the LSB systems are typed S*cd* or later. The central disk surface brightnesses are similar for bulge and non-bulge HSB systems.

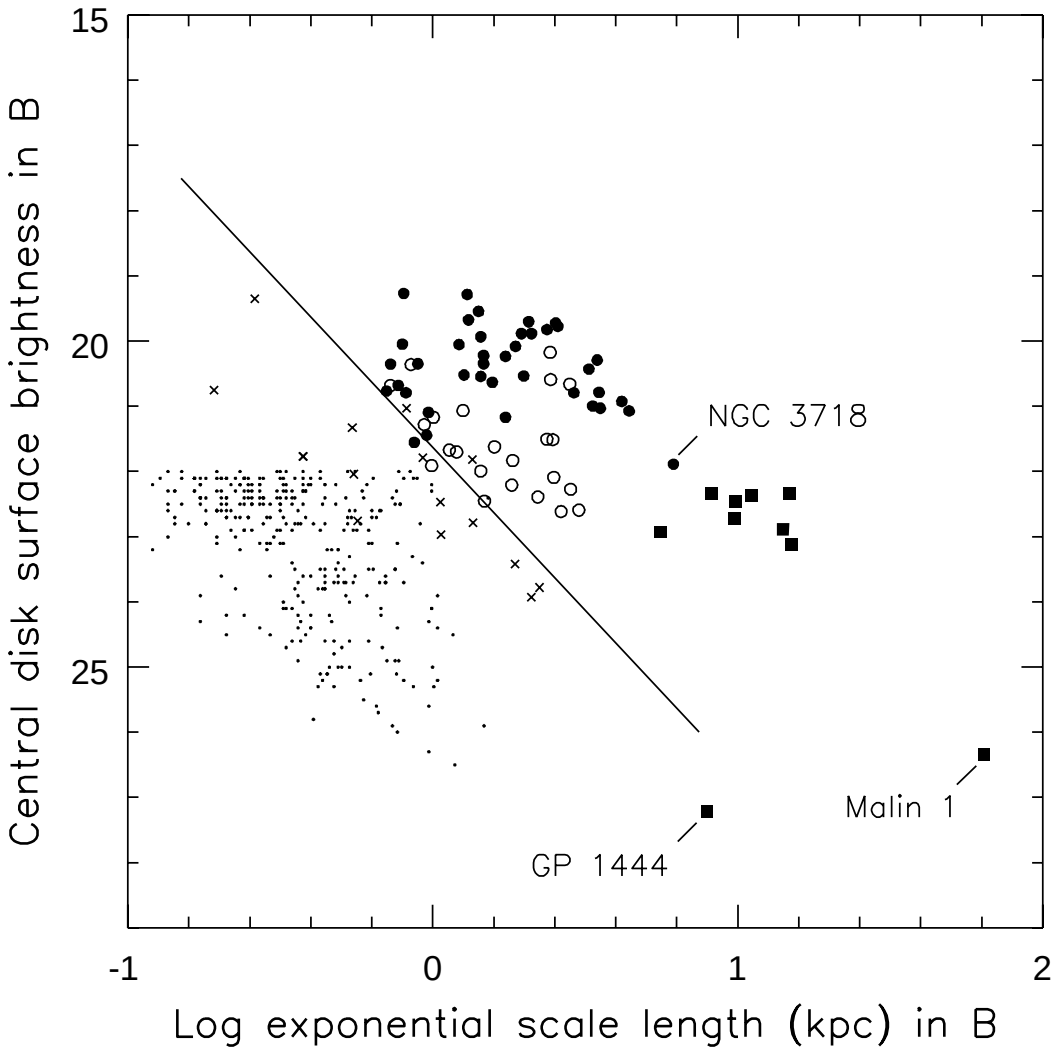

Figure 7: Comparison with $\mu_0 - r_d$ information from the literature. Data is in B-band without inclination adjustments to make the broadest comparison. The circles and straight line are the same information shown in Fig. 1 (B panel) except the HSB and LSB galaxies are now filled and open symbols, respectively. The small dots locate the low surface brightness galaxies cataloged in the direction of the Fornax Cluster by Davies et al. (1988*a*) and Irwin et al. (1990). The points are plotted assuming Fornax is 11% more distant than Ursa Major. There is confusion from background contamination for the shorter scale length objects with $22 < \mu_0 \lesssim 23$ but most of the fainter surface brightness objects should be in the Fornax Cluster. The large filled squares identify the 'giant' low surface brightness spiral galaxies studied by Sprayberry et al. (1995) plus the two extreme systems Malin 1 (Bothun et al. 1987) and GP 1444 (Davies et al. 1988*b*). The unusual galaxy NGC 3718 is identified in the figure.

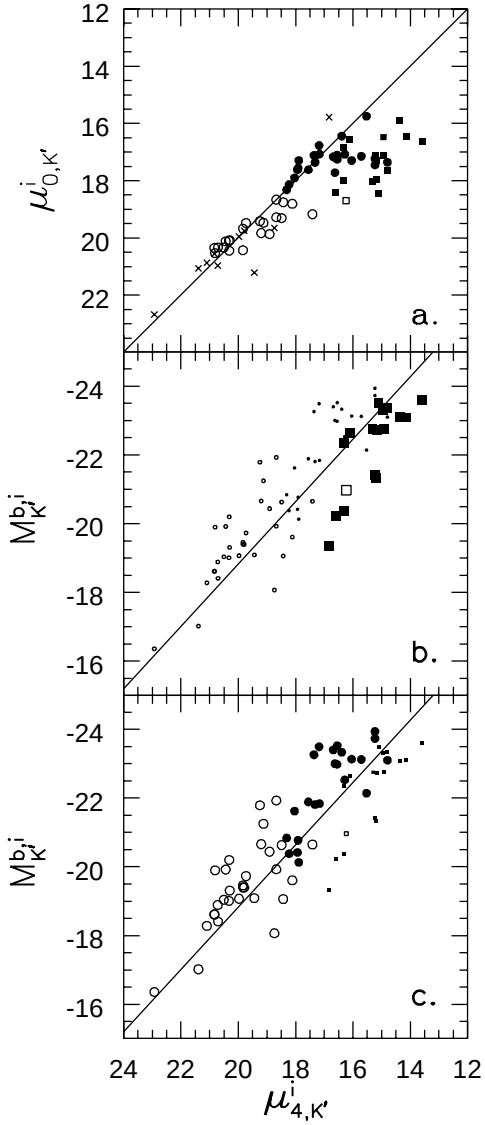

Figure 8: Correlations with the K' surface brightness within $4'' = 300$ pc of the center of galaxies. (a) Comparison of the inclination corrected exponential disk central surface brightness, μ_0^i, and the inclination corrected surface brightness of the bulge plus disk in the central $4''$, μ_4^i. HSB: filled symbols; LSB: open symbols; $T \leq 2$: boxes; $T \geq 3$: circles; galaxies not in the complete sample: crosses. The galaxies with substantial bulges ($\mu_4^i \ll \mu_0^i$) almost all have types $\leq$ Sab. (b) Correlation between μ_4^i and absolute magnitude at K' with emphasis on early types. Filled symbols: HSB; open symbols: LSB; big squares: type $\leq$ Sab; little circles: type $\geq$ Sb. The straight line is the regression on *all* galaxies which minimizes the scatter in μ_4^i. The one open square is for NGC 4117, nominally LSB. The only square to the left of the regression line for the entire sample is NGC 3729, the galaxy interacting with NGC 3718 and typed Sab. (c) Same as panel b but with emphasis on late types. Now circles are big and squares are small.

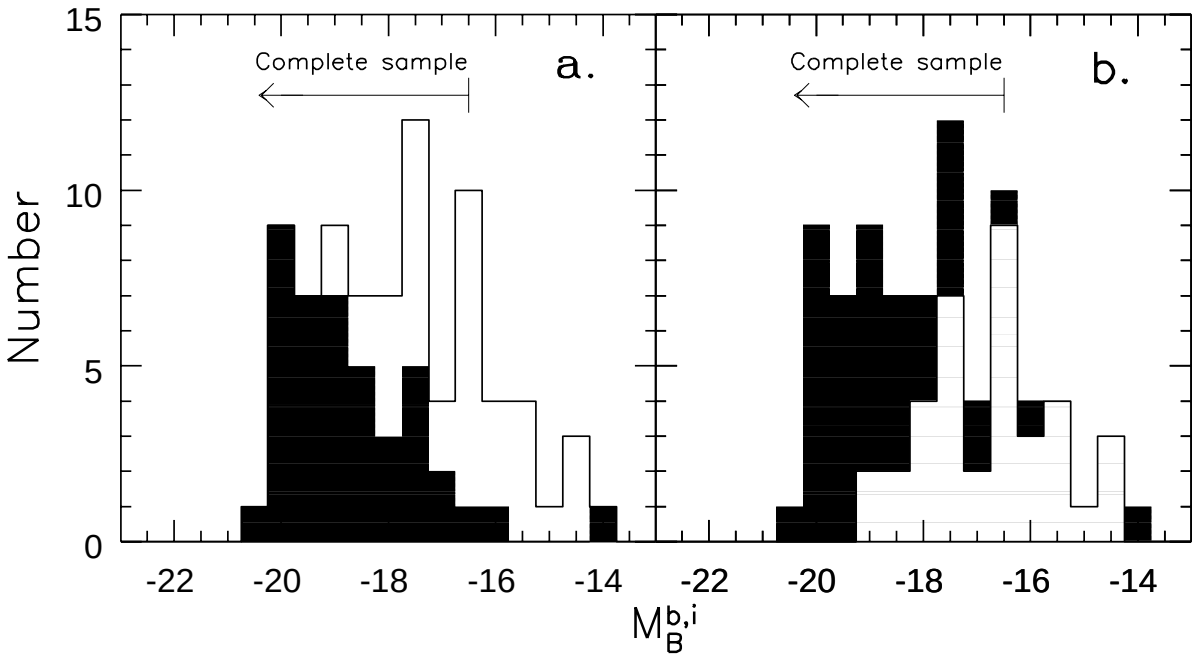

Figure 9: Luminosity functions in B-band. (a) The HSB sub-sample is shaded and embedded in the luminosity function for the entire sample. There is completion to $M_B^{b,i} = -16.5^m$. The cutoff of the HSB luminosity function by $M_B^{b,i} \sim -17^m$ is unlikely to be an observational artifact. (b) The LSB sub-sample is shown as an open histogram embedded in the ensemble function. The LSB component begins at $M_B^{b,i} \sim -19^m$ and rises steeply to the completion limit.

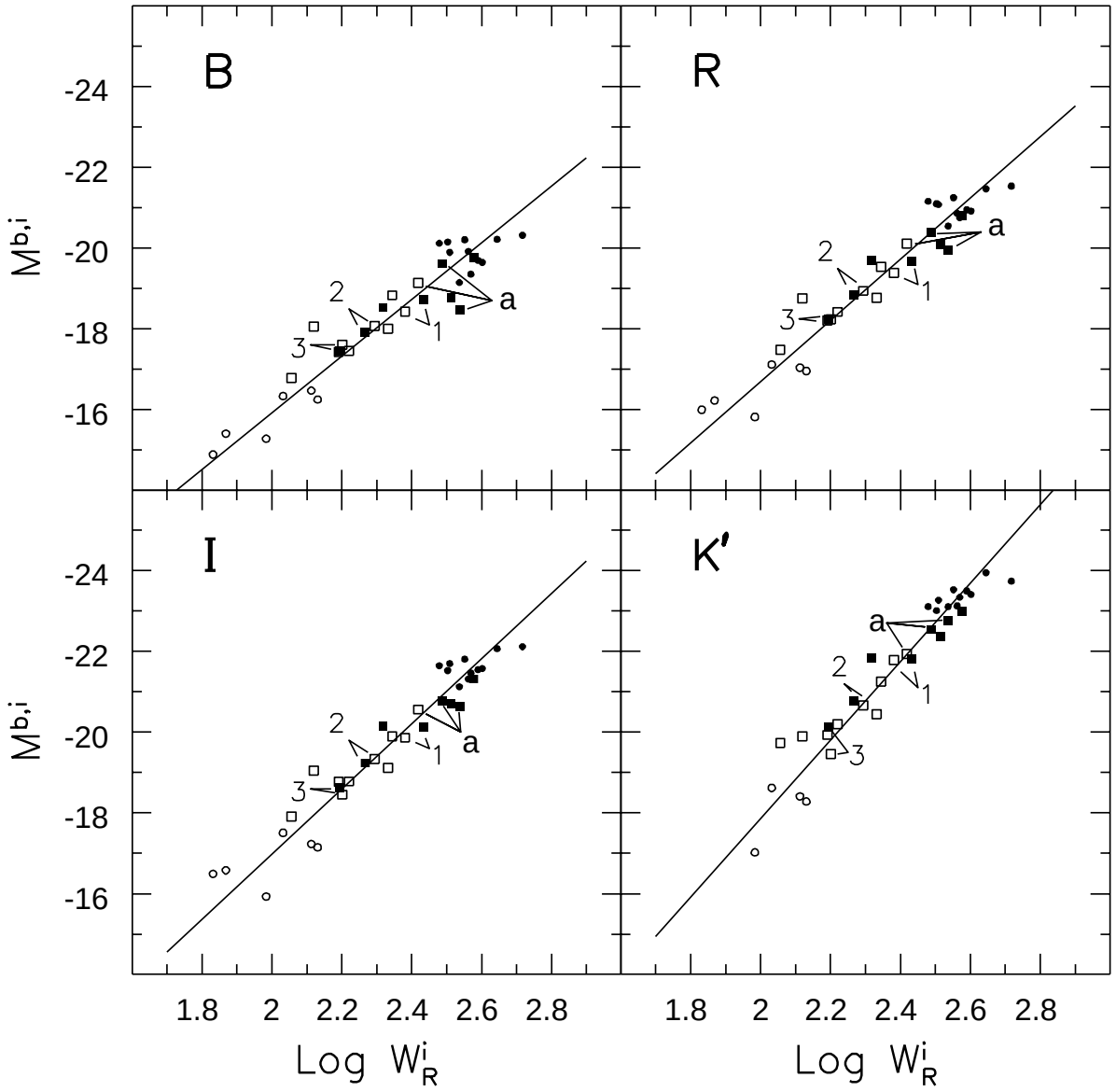

Figure 10: Luminosity–line width correlations are shown for 34 galaxies in the four passbands. HSB: filled symbols; LSB: open symbols. Galaxies in the overlap region $-23^m < M^{b,i}_{K'} < -19^m$ ($-19^m < M^{b,i}_B < -17^m$) are indicated by box symbols. Three pairs and a triplet given special attention are noted by labels 1,2,3 and a. The straight lines are regressions which minimize scatter in line widths.

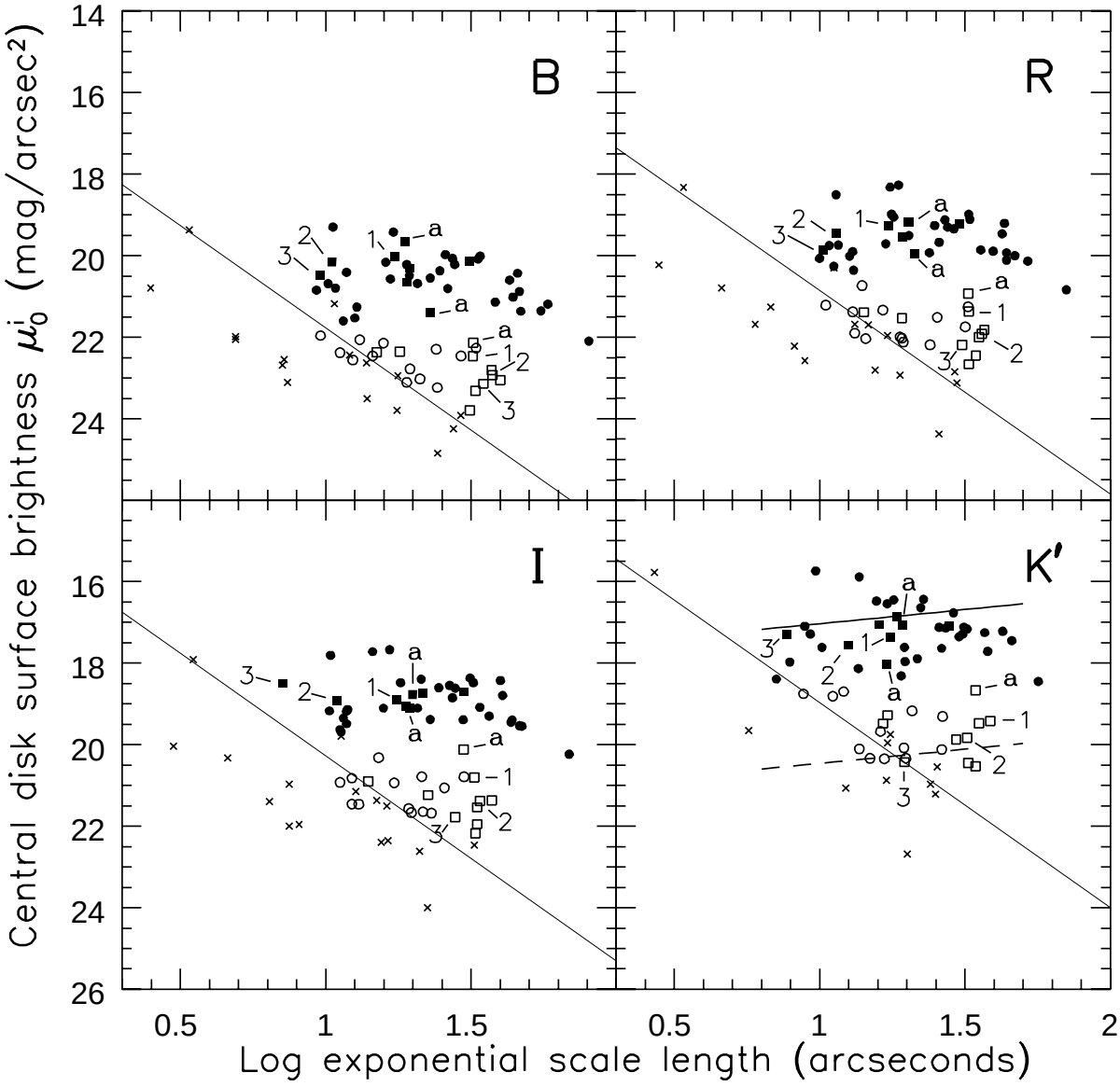

Figure 11: Repetition of Fig. 3 except the galaxies identified with box symbols in Fig. 10 are identified with the same symbols here. Small HSB galaxies and large LSB galaxies with similar luminosities also have similar maximum rotation velocities. Three pairs and a triplet given special attention are identified as in Fig. 10. In the K' panel, the solid line is the locus of the relation $V_{max}^{disk}/0.5W_R^i = 2/3$ while the dashed line correspondes to $V_{max}^{disk}/0.5W_R^i = 1/3$.

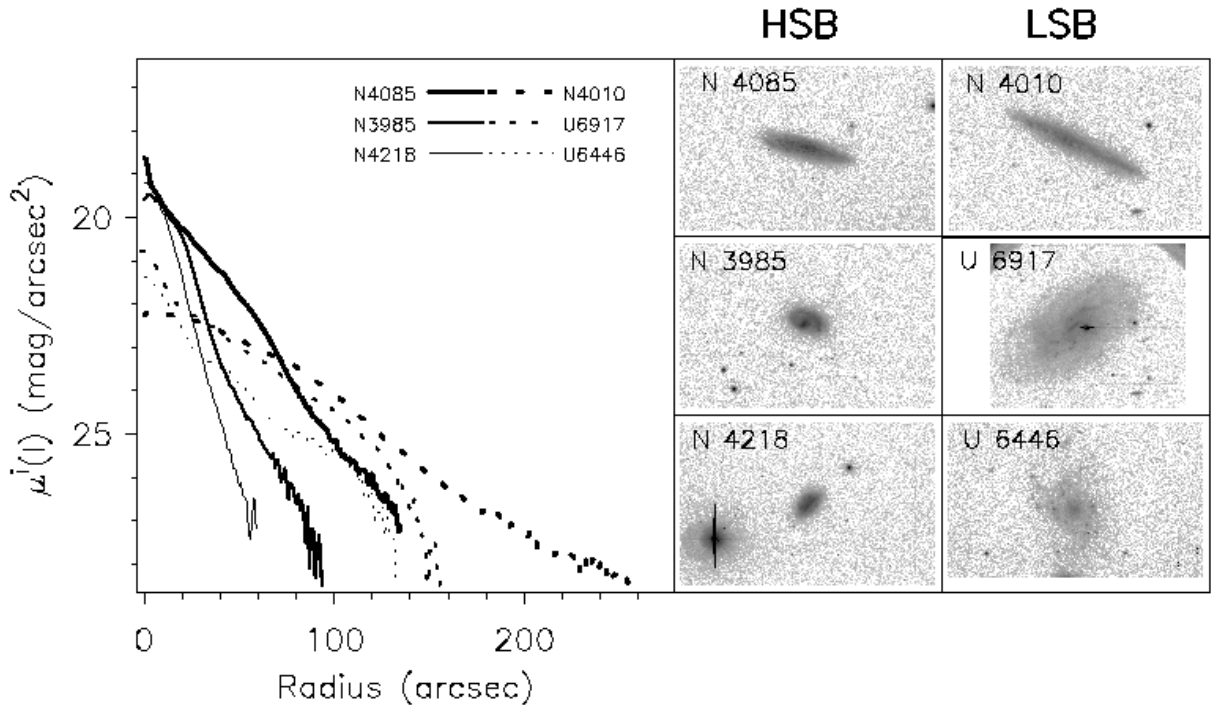

Figure 12: I-band inclination adjusted surface brightness versus radius for the three HSB–LSB pairs of galaxies identified in Figs. 10 and 11. The B images of the pairs are shown in the inset at common scales. Pair 1: NGC 4085/NGC 4010. Pair 2: NGC 3985/UGC 6917. Pair 3: NGC 4218/UGC 6446.

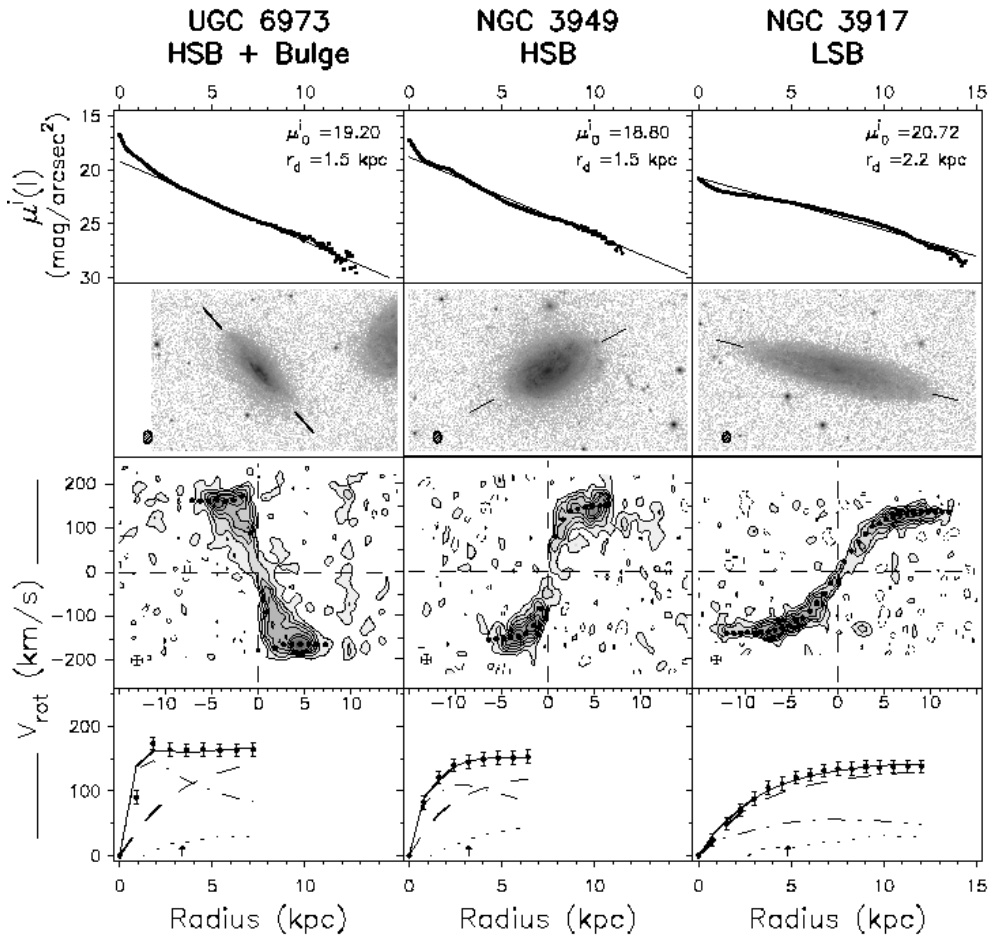

Figure 13: Rotation curve decompositions. Examples of the three distinct classes of disk galaxies are presented in each of the vertical groups. On the left is UGC 6973, a system with a HSB exponential disk and a central bulge. In the middle is NGC 3949, a system with a HSB disk but no appreciable bulge. On the right is NGC 3917, a system with a LSB disk and no bulge. In each case, the horizontal axes are position in kpc. In the top and bottom panels the origin with respect to the nucleus is at the left axis, while in the middle panels the origin with respect to the nucleus is at the center of the plots. Surface brightnesses at I, corrected for inclination, are shown in the top panels. Images at B are shown in the second row. The major axes are indicated, as well as the FWHM beam of the HI observations. The velocity-position decomposition of the HI observations is seen in the panels of the third row. Velocities averaged over annuli are given as dots. The rotation curve decompositions are provided in the bottom panels. The solid lines with error bars illustrate the observed rotation curves. Dot–dashed curves illustrate the amplitude of rotation expected from the observed distributions of light and $M/L = 0.4$ at K'. The dotted curves illustrate the contribution expected from the gas component. The dashed curves demonstrate the residual contribution attributed to a dark matter halo. Isothermal spheres are used in this modelling.

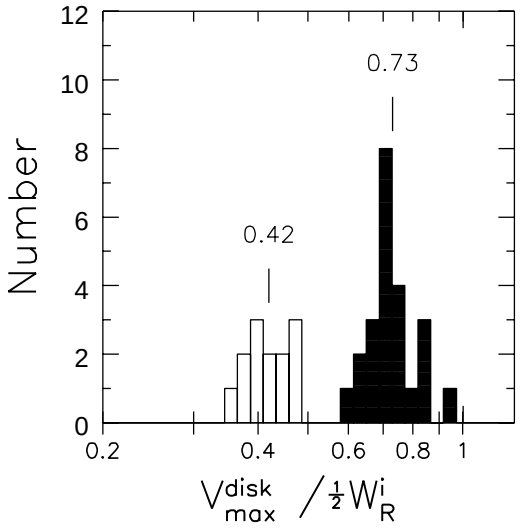

Figure 14: Histogram of the ratio $V_{max}^{disk}/0.5W_R^i$ based on photometric properties. Isolated sub-sample only (nearest important neighbor > 80 kpc in projection). Values of V_{max}^{disk} follow from the properties of the exponential disk and $M/L_{K'} = 0.4M_\odot/L_\odot$. The relation between W_R^i and photometric parameters is given by the luminosity–line width correlation. Filled histogram: HSB systems; open histogram: LSB systems. Mean values for each family are indicated.